Transportation Research Part E 206 (2026) 104558

Contents lists available at ScienceDirect

Transportation Research Part E

journal homepage: www.elsevier.com/locate/tre

Dynamic multimodal transport planning with drones for emergency logistics: Mathematical model and heuristic algorithm

Yimeng Zhang [a,b,c,d], Shuyang Zhu [a], Kaiyu Pu [a], Hang Cui [e], Mi Gan [a,b,*], Xiaobo Liu [a,b], Ruixue Ai [f]

[a] School of Transportation & Logistics, Southwest Jiaotong University, Chengdu, China
[b] National Engineering Laboratory of Integrated Transportation Big Data Application Technology, Southwest Jiaotong University, Chengdu, China
[c] Tangshan Institute, Southwest Jiaotong University, Tangshan, China
[d] Department of Transport & Planning, Delft University of Technology, Delft, the Netherlands
[e] School of Architecture, Southwest Jiaotong University, Chengdu, China
[f] University of Oslo, Oslo, Norway

ARTICLE INFO

Keywords:
Emergency logistics
Multimodal transport
Dual-role drones
Dynamic transport planning
Adaptive large neighborhood search

ABSTRACT

Dynamic multimodal transport planning is vital for enhancing flexibility and responsiveness in emergency logistics. We propose a dynamic planning approach that integrates drones into the multimodal system with trains, trucks, and aircraft, introducing dual-role drones that can be transported as cargo and later operate as carriers. A Mixed Integer Programming (MIP) model, optimized via a rolling horizon approach, supports real-time route planning. Given the problem's complexity, we develop an Adaptive Large Neighborhood Search (ALNS) algorithm with problem-specific operators. The model accounts for mode coordination, routing constraints, and cargo heterogeneity. It dynamically replans routes under disruptions such as road damage, considering mode availability and delivery requirements. Numerical experiments are conducted based on a real disaster scenario. A comparison with an exact method shows improved computational efficiency and solution quality. Further comparisons with a drone-free and static approach highlight gains in service rate and disruption resilience. We also examine the impact of cargo heterogeneity. These results, across instances from 5 to 400 orders, provide practical insights for optimizing drone deployment, transport mode selection, and cargo management in disaster response.

1. Introduction

The frequent occurrence of natural disasters–such as tsunamis, hurricanes, and earthquakes–continues to pose major challenges worldwide (Meng et al., 2023). In 2024, 393 global disasters resulted in 16,753 deaths, affected over 167 million people, and led to $242 billion in losses (The International Disaster Database, 2025). On May 28, 2025, the Mokwa flood devastated the Nigerian town of Mokwa, killing at least 500 people, leaving more than 600 people missing, injuring 200, and destroying over 4000 homes (Wikipedia, 2025). These figures highlight the urgent need for efficient emergency logistics systems to reduce human and economic losses. Such systems must support dynamic planning and coordinate multiple transport modes to meet diverse and urgent demands, especially when infrastructure is severely damaged (Jiang and Yuan, 2019; Yi and Kumar, 2007; Abdelgawad and Abdulhai, 2009; Wang et al., 2015; Meng et al., 2023; Zhang et al., 2025).

* Corresponding author at: Southwest Jiaotong University, No. 999, Xi'an Road, Pidu District, Chengdu, Sichuan, PR China.
E-mail address: migan@swjtu.edu.cn (M. Gan).

https://doi.org/10.1016/j.tre.2025.104558
Received 29 April 2025; Received in revised form 27 August 2025; Accepted 16 November 2025

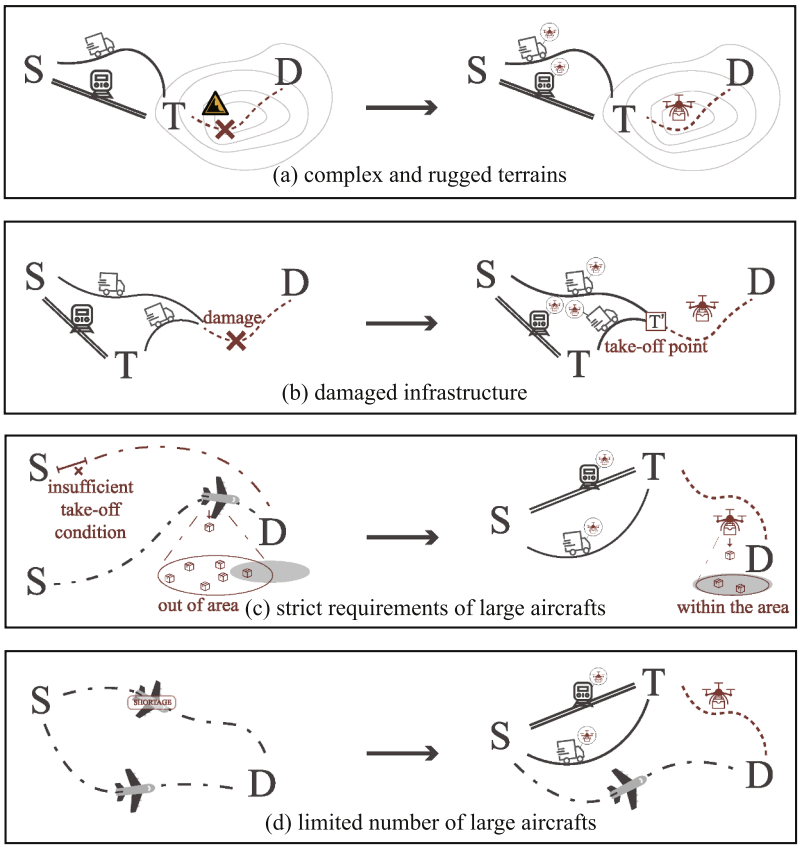

Fig. 1. The advantages of drones in emergency logistics compared to traditional transport modes.

Multimodal transport enhances the efficient and precise delivery of emergency supplies, offering flexibility and adaptability in complex environments to boost logistics performance and response speed (Maghfiroh and Hanaoka, 2020; Meng et al., 2023). Traditional modes–trucks, trains, cargo aircraft, and ships–have long been studied and applied in emergency logistics (Özdamar et al., 2004; Vitoriano et al., 2009; Salmerón and Apte, 2010; Zhang et al., 2019; Xiong et al., 2019; Maghfiroh and Hanaoka, 2020; Zhang et al., 2022c; Meng et al., 2023; Rodríguez-Espíndola et al., 2023). More recently, drones have gained attention for their exceptional flexibility (Nedjati, 2017; Fikar et al., 2016). Operating independently of road and rail networks, drones can overcome logistical barriers and ensure high-precision deliveries. As shown in Fig. 1, drones can navigate rugged terrains–mountains, forests, and urban ruins (Fig. 1(a))–and bypass damaged infrastructure like broken roads or blocked railways (Fig. 1(b)) (Shi et al., 2024). Unlike large aircraft, which require long runways and face limitations in accurate delivery due to altitude and maneuverability, drones can launch from vehicles, land almost anywhere, and deliver supplies directly to target locations–even in complex environments (Fig. 1(c)). Their widespread availability also offsets the limited supply of large aircraft, enhancing scalability when integrated into multimodal systems (Fig. 1(d)). These capabilities make drones a vital innovation in emergency logistics, enabling smarter resource allocation and faster, more effective disaster response.

Previous studies have leveraged drone flexibility by coordinating them with trucks (Otto et al., 2018; Rojas Viloria et al., 2021; Zhou et al., 2023; Shi et al., 2024), but few have explored drone integration into broader multimodal emergency logistics systems. This paper fills that gap by proposing a dynamic multimodal transport optimization model incorporating roads, railways, large cargo aircraft, and drones. In this model, drones play a dual role: they are first transported by other modes to designated takeoff points or areas near damaged infrastructure, then switch to a carrier role to deliver supplies directly to demand points–enabling rapid and precise relief in dynamic conditions. When feasible, roads, railways, and aircraft can also deliver cargo directly. The contributions of this study include: (a) Developing a Mixed Integer Programming (MIP) model for Dynamic Multimodal Transport with Dual-Role Drones (DMT-Drones), combining the long-range efficiency of conventional modes with the precision and adaptability of drones in complex environments. (b) Introducing an Adaptive Large Neighborhood Search (ALNS) heuristic to significantly reduce computation time and improve practical usability. (c) Proposing a rolling horizon approach for real-time adaptability, allowing drone and other vehicles' paths to dynamically respond to disruptions such as infrastructure damage. (d) Providing managerial insights through extensive experiments under varying drone usage levels, road conditions, and heterogeneous demand scenarios.

The remainder of this paper is organized as follows: Section 2 presents a concise review of the literature on multimodal transport planning in emergency logistics and vehicle routing with drones. Section 3 provides a detailed problem description. Section 4 intro-

duces the rolling horizon approach for dynamic planning. The optimization problem is formulated as an MIP model in Section 5. Section 6 outlines the solution methodology, detailing a customized ALNS algorithm with specialized operators and performance improvements. Section 7 reports the experimental design and results. Finally, Section 8 concludes the paper and discusses future research directions.

2. Literature review

Section 2.1 reviews the literature on multimodal transport planning for emergency logistics. This is followed by an analysis of research focusing on the coordination between drones and trucks in Section 2.2. Finally, Section 2.3 concludes with a summary that highlights the research gaps.

2.1. Multimodal transport planning for emergency logistics

An increasing number of studies have studied multimodal transport planning for emergency logistics (Veysmoradi et al., 2018; Ruan et al., 2018; Xiong et al., 2019; Gao et al., 2021; Meng et al., 2023; Beiki Ashkezari et al., 2024; Xu et al., 2024; Zhang and Lu, 2024; Yin et al., 2024a). For example, Xiong et al. (2019) model helicopters and vehicles as interdependent subsystems, optimizing them separately before integrating the results. Ruan et al. (2018), Gao et al. (2021) and Yin et al. (2024b) tailor their models to mode-specific characteristics to improve overall system performance. Yin et al. (2024b) develop a two-stage recoverable robust optimization model integrating facility location, relief delivery by trucks via ground networks, and casualty transfer by helicopters via air routes within a multimodal transport framework under various uncertainty scenarios. Meng et al. (2023), Beiki Ashkezari et al. (2024), and Xu et al. (2024) integrate air, rail, and road transport modes, leveraging the advantages of each to minimize the delivery time and the transport cost in emergency logistics operations. While drones have been studied for monitoring (Nedjati, 2017) and aerial delivery (Fikar et al., 2016), they are often treated in isolation, with limited integration into multimodal systems. This limits their potential to complement traditional modes (e.g., by navigating inaccessible areas and reducing response times) and highlights a key gap in current research.

Dynamic optimization remains underexplored. Most existing models are static and do not adapt to real-time changes in disaster scenarios (Zhang et al., 2019; Maghfiroh and Hanaoka, 2020; Xiong et al., 2019; Rodríguez-Espíndola et al., 2023; Beiki Ashkezari et al., 2024; Xu et al., 2024; Yin et al., 2024b). Some early efforts, e.g., Özdamar et al. (2004) and subsequent extensions (Yi and Kumar, 2007; Abdelgawad and Abdulhai, 2009; Wang et al., 2015), introduce dynamic models for real-time material allocation and routing. More recently, Ruan et al. (2018) and Zhang and Lu (2024) have addressed dynamic environments, including a truck-drone routing problem using multi-agent deep reinforcement learning. However, few models dynamically integrate drones with other transport modes. In disrupted settings, dynamically adjusting drone takeoff points to bypass damaged infrastructure offers untapped potential for maintaining delivery continuity–an area still largely unexplored.

Cargo heterogeneity has also received limited attention. While some studies examine multi-commodity transport (Liu et al., 2019; Zhang and Lu, 2024), few address diverse cargo characteristics (Hu, 2011; Yi and Kumar, 2007; Wang et al., 2015).

In summary, current research on multimodal transport planning for emergency logistics still faces key gaps. The integration of drones with traditional modes remains limited, preventing full utilization of their complementary strengths. While progress has been made in dynamic optimization, real-time adaptability (especially in adjusting drone takeoff points during infrastructure disruptions) remains underdeveloped. Additionally, cargo heterogeneity is often overlooked, with insufficient consideration of varying cargo types, sizes, and priorities. Addressing these gaps is essential to improving the resilience, responsiveness, and overall efficiency of multimodal emergency logistics systems.

2.2. Vehicle routing problem with drones

The Vehicle Routing Problem with Drones (VRPD) integrates trucks and drones for coordinated deliveries, where drones accompany trucks, serve customers, and can transfer between trucks at service centers–leveraging truck capacity and drone flexibility for synergistic efficiency (Schermer et al., 2019). Leading companies such as Amazon, Walmart, Google, Alibaba, DHL, and SF Express have adopted such systems (Shi et al., 2024). Murray and Chu (2015) introduce the Flying Sidekick Traveling Salesman Problem (FSTSP), proposing a heuristic that considers drone endurance and load limits. Building on this, Agatz et al. (2018) develop the Traveling Salesman Problem with Drone (TSP-D), focusing on drone returns to the same location, while Ha et al. (2020) use this framework to minimize total costs, including transport and waiting times. Further advances include a VNS-based approach by de Freitas and Penna (2020) and a two-stage MIP model with Benders decomposition by Vásquez et al. (2021), though these largely focus on single-truck-single-drone scenarios.

Expanding beyond this, Tu et al. (2018) and Moshref-Javadi et al. (2020) propose single-truck-multiple-drone (TSP-MD) models, enhancing operational flexibility. Murray and Raj (2020) extend FSTSP to account for drone-specific constraints such as varying speeds, payloads, and flight times. Similarly, Poikonen and Golden (2020) and Gómez-Lagos et al. (2021) develop heuristic and MIP-based solutions for TSP-MD problems.

Beyond single-truck systems, Wang and Sheu (2019) extend VRPD to multi-vehicle settings using a branch-and-price algorithm, showing that truck-drone collaboration reduces delivery time under complex conditions. Shi et al. (2024) address emergency logistics with an MIP model and two-stage heuristic for dispatching drones, cargo aircraft, and trucks. Wu et al. (2024) tackle truck-drone routing for medical deliveries during a pandemic, employing a Multi-Objective Snow Goose Algorithm. However, their study has

several limitations: (a) it lacks dynamic planning, (b) it excludes multimodal integration, and (c) it assumes a single distribution center.

Several studies adopt exact algorithms to solve various truck–drone routing problems. Yin et al. (2024a) develop an exact integer L-shaped method integrating Benders decomposition (BD) and branch-and-price (BP) to solve a vehicle–drone cooperative delivery routing problem for blood product distribution. Yin et al. (2025) focus on pickup and delivery with availability profiles using a branch-and-price-cut (BPC) framework enhanced by column-and-cut generation and bidirectional labeling. Li et al. (2024) address simultaneous delivery and pickup with time windows via a set-partitioning-based BPC algorithm. Yin et al. (2023) solve a robust VRP with drones under demand and travel time uncertainty using a BPC approach tailored with bounded bidirectional labeling. Meanwhile, some studies consider uncertainty in emergency logistics. Peng et al. (2025) formulate a Markov game model under dynamic uncertainty of demand and location and solve it using multi-agent deep reinforcement learning. Wang et al. (2025) address a stochastic truck–drone VRP using a hybrid SISRs and greedy insertion algorithm. Xin et al. (2025) develop a two-stage distributionally robust optimization model for humanitarian logistics network design under incomplete demand information. Among these works, Wu et al. (2024) address the optimization problem with a single distribution center, Wang et al. (2025) and Shi et al. (2024) examine truck–drone systems with exactly one drone per truck, whereas Peng et al. (2025) and Yin et al. (2024a) restrict each drone to serving only one affected location per trip. Several studies focus primarily on exact approach and conduct experiments on small-scale scenarios (Peng et al., 2025; Yin et al., 2025, 2024a). Notably, with the exception of Peng et al. (2025), dynamic planning is not explicitly addressed. Moreover, aspects such as cargo heterogeneity and the integration of multiple transport modes (e.g., trains and helicopters) are generally less emphasized, despite their importance for effective emergency logistics.

In summary, existing research on drone-truck coordination mainly targets commercial parcel delivery, with limited application in emergency logistics and minimal integration of other transport modes such as rail and air (Wu et al., 2024). This study advances the field by integrating trucks, drones, railways, and large aircraft in a multi-mode, multi-drone optimization framework, aiming to improve resource allocation and enhance emergency response efficiency.

2.3. Summary

Table 1 summarizes studies on multimodal transport planning for emergency logistics and VRPD. While notable progress has been made in multimodal emergency logistics, no existing studies incorporate drone coordination within broader multimodal systems. Most rely on static models (Rodríguez-Espíndola et al., 2023; Veysmoradi et al., 2018; Xiong et al., 2019; Zhang et al., 2019; Maghfiroh and Hanaoka, 2020; Ertem et al., 2022; Meng et al., 2023), which overlook the dynamic disruptions common in disaster scenarios. Cargo heterogeneity is also frequently neglected, especially in complex environments like mountainous regions (Zhang et al., 2019; Maghfiroh and Hanaoka, 2020; Xiong et al., 2019; Veysmoradi et al., 2018; Ruan et al., 2018; Meng et al., 2023; Ertem et al., 2022; Wang et al., 2015).

In the VRPD literature, most studies concentrate on the FSTSP (Murray and Chu, 2015; Agatz et al., 2018; Vásquez et al., 2021), with limited attention to multi-drone or multi-truck scenarios such as mFSTSP and extended VRPD models (Tu et al., 2018; Murray and Raj, 2020; Wang and Sheu, 2019). These works seldom explore multimodal coordination or account for cargo diversity. While some incorporate dynamic modeling (Agatz et al., 2018), most assume fixed drone takeoff points, lacking the flexibility to adapt to emergent conditions–an essential capability in real-world emergency logistics.

The study most closely related to this work is Shi et al. (2024), which focuses on post-disaster material scheduling using aircraft-truck-drone coordination. However, this study introduces several key advancements: (a) Unlike Shi et al. (2024), which models routing as a variant of the Traveling Salesman Problem without considering drone coordination within multimodal transport, this study emphasizes the essential role of drones in addressing the limitations of traditional multimodal systems. (b) While Shi et al. (2024) present only small-scale experiments and exclude trains, this study includes large-scale scenarios and incorporates train-based logistics. (c) Shi et al. (2024) assume a static environment and ignore cargo heterogeneity; in contrast, this study accounts for dynamic road disruptions and diverse cargo types, leveraging drones' adaptability. (d) Methodologically, Shi et al. (2024) use a Tabu Search algorithm, whereas this study adopts the more adaptive ALNS algorithm for improved solution quality and scalability.

3. Problem description

All notations utilized in our study are presented in Table 2.

In this study, we utilize three transport modes–flight (f), road (h), and rail (r)–coordinated with drones (u) for emergency logistics, represented by the mode set $W = \{f, h, r, u\}$. Each mode $w \in W$ has a corresponding vehicle set indexed by K_w. Routes and timetables for all modes, except K_r, are flexible. Drones (k_u) have dual roles: they are initially transported as cargo (o_u) to designated transfer or takeoff points, after which they act as active carriers (k_u). Therefore, drones are treated as a distinct mode with dual functionality rather than purely aerial transport.

The cargo types handled by vehicles k include normal relief supplies (o_n), emergency relief supplies (o_e), and drone units (o_u). Normal relief supplies (o_n) include bulky, heavy items such as food staples (e.g., rice, flour), large medical equipment (e.g., CT machines), and construction materials (e.g., steel, cement), which are crucial for long-term support but less time-sensitive. In contrast, emergency relief supplies (o_e) consist of lightweight, high-priority items such as medications, compressed food, and communication devices, requiring rapid delivery to meet immediate post-disaster needs. The number of drones assigned to each vehicle group is not predetermined; instead, it is determined dynamically through the optimization process based on vehicle capacity constraints and task requirements. This allows the model to flexibly adapt to different disaster scenarios, enhancing its practicality, generalization

Table 1
Literature review on multimodal emergency logistics and vehicle-drone routing.

	Characteristic					Model approach		
Literature	Modes	Problem	Cargo heterogeneity	Transfer	Objective	Dynamics	Modeling approach	Solution algorithm
Multimodal emergency logistics								
Veysmoradi et al. (2018)	A, H	MELO-U		✓	c, t, r		MINLP	RO
Ruan et al. (2018)	A, H	MELO-UTC		✓	t, r	RP	MIP	GA
Zhang et al. (2019)	A, H, R	MELO-SD			c, t, u		SP	FMO
Xiong et al. (2019)	A, H	mLPR		✓	t		LP	HHA
Maghfiroh and Hanaoka (2020)	A, H, R, W	MELO		✓	c, t		MIP	BC
Ertem et al. (2022)	H, R, W	MELO		✓	u, t		NFM	RA
Meng et al. (2023)	A, H, R	MELO-DU		✓	c, t		SP	EA
Rodríguez-Espíndola et al. (2023)	A, H, R, W	MELO		✓	c, s		SP	ϵ
Beiki Ashkezari et al. (2024)	A, H, R	MELO-U		✓	c, t		MILP	CPLEX
Xu et al. (2024)	A, H, R	MELO-UC		✓	c, t		MIP	GA, PSO
Zhang and Lu (2024)	A, W	MELO-TV-MRCS		✓	c, l		MINLP	PSO-PGSA
Yin et al. (2024b)	A, H	MELO-LAEP		✓	c		MILP	CCG, BDA
Vehicle-drone routing								
Ha et al. (2020)	H, U	TSPD		✓	c		IP	LS, GRASP
Murray and Raj (2020)	H, U	mFSTSP		✓	c, t		MIP	He
de Freitas and Penna (2020)	H, U	FSTSP		✓	t		MIP	GVNS
Vásquez et al. (2021)	H, U	TSPD		✓	c		MIP	BDA
Gómez-Lagos et al. (2021)	H, U	TSPD		✓	t		MIP	GRASP
Yin et al. (2023)	H, U	RVRPD		✓	c		MILP	BPC
Shi et al. (2024)	A, H, U	MDVRPD-H		✓	t		MIP	TSA
Wu et al. (2024)	H, U	VRPD		✓	c, t, d		MOCC	EDA-MOSGA
Li et al. (2024)	H, U	VRPSDP-TDH		✓	c		MILP	BPC
Yin et al. (2024a)	H, U	VDCDRP-BP		✓	c, u		A-MICP	BP, BDA
Peng et al. (2025)	H, U	D-VRPD		✓	c	Event-RL	MG, MIP	MADRL
Yin et al. (2025)	H, U	PDP-AP		✓	c		MILP	BPC, CCG GI, SA,
Wang et al. (2025)	H, U	TDRP-SD		✓	c		MIP	SISRs, SRDS
Xin et al. (2025)	H, U	FLIP-TDS	✓		c		MILP	DA
This article	A, H, R, U	DMT-Drones	✓	✓	c	RH-E	MIP	ALNS

Modes : A: Aviation; H: Road; R: Railway; W: Waterway; U:drone.
Problem : MELO-U: Multimodal emergency logistics optimization considering uncertainty; MELO-UTC: Multimodal emergency logistics optimization considering updated transfer centers; MELO-SD: Multimodal emergency logistics optimization considering secondary disasters; mLPR: multi-level location-routing problem; MELO-DU: Multimodal emergency logistics optimization considering dynamic uncertainty; MELO-UC: Multimodal emergency logistics optimization under uncertain conditions; MELO-TV-MRCS: Multimodal emergency logistics optimization with time–varying multi–resource collaborative scheduling; MELO-LAEP: emergency logistics optimization with location–allocation and evacuation planning problem; TSPD: Traveling salesman problem with drones; mFSTSP: Multiple flying sidekicks traveling salesman problem; FSTSP: Flying Sidekick Traveling Salesman Problem; RVRPD: Robust vehicle routing with drones; MDVRPD-H: Multi-Depot Vehicle Routing Problem with drones and cargo aircraft; VRPD: Vehicle routing problem with drones; VRPSDP-TDH: Truck-drone Routing Problem with Simultaneous Delivery and Pickup and Heterogeneous Drones; VDCDRP-BP: Vehicle-and-drone cooperative delivery routing problem of blood products; D-VRPD: Dynamic vehicle routing problem with drones; PDP-AP: Pickup and Delivery Problem with Availability Profiles; TDRP-SD: Truck–drone Routing Problem with Stochastic Demand; FLIP-TDS: Facility Location and relief supply Inventory Pre-positioning problem with Truck-Drone Support; DMT-Drones: Dynamic multimodal transport with dual-role drones.
Objective : c: minimize the cost; t: minimize the time; r: maximize the reliability; u: minimize the unsatisfied demand; s: minimize the shortage of relief; l: minimize the loss; d: minimize the discrepancy.
Dynamics : RH-E: Event-triggered rolling horizon; RP: Re-planning; Event-RL: Event-driven based reinforcement learning.
Modeling approach : MINLP: Mixed-Integer Nonlinear Programming; MIP: Mixed Integer Programming; SP: Stochastic Programming; LP: Linear Programming; NFM: Network Flow Model; MILP: Mixed-Integer Linear Programming; IP: Integer Programming; MOCC: Multi-objective Chance-constrained Model; A-MICP: Arc-based mixed integer convex programme; MG: Markov Game.
Solution algorithem : RO: Robust Optimization; GA: Genetic Algorithm; FMO: Fuzzy Multi-objective Optimization; HHA: Hybrid Heuristic Algorithm; BC: Branch and Cut; RA: Retrospective Analysis; EA: Evolutionary Algorithm; ϵ: ϵ - Constraint; CPLEX: IBM ILOG CPLEX; PSO: Particle Swarm Optimization; PSO-PGSA: Particle Swarm Optimization based Plant Growth Simulation Algorithm; CCG: Column-and-Constraint Generation; BDA: Benders Decomposition Algorithm; LS: Local Search; GRASP: Greedy Randomized Adaptive Search Procedure; He: Heuristic; DP: Dynamic Programming; GVNS: General Variable Neighborhood Search; BPC: Branch-Price-and-Cut; TSA: Tabu Search Algorithm; EDA-MOSGA: Estimation of Distribution Algorithm combined with Multi-objective Snow Goose Algorithm; BP: Branch-and-Price; MADRL: Multi-agent Deep Reinforcement Learning; GI: Greedy Insertion; SA: Simulated Annealing; SISRs: Slack Induction by String Removals; SRDS: Short-route Deep Search; DA: Decomposition Algorithm; ALNS: Adaptive Large Neighborhood Search.

Table 2
Notation.

Sets:	
W	Set of modes indexed by w. $W = \{f, h, r, u\}$, where f stands for flight transport, h for road transport, r for rail transport, and u for drones in its carrier state.
O	Set of orders indexed by o. $O = O_n \cup O_e \cup O_u$, O_n for set of orders with normal rescue cargo indexed by o_n, O_e for set of orders with emergency rescue cargo indexed by o_e, O_u for set of drones in its order state indexed by o_u.
N	Set of locations indexed by i and j. $S/D/T/T'/B \subseteq N$, set of supply/demand/transfer/takeoff/disruption points.
K	Set of vehicles indexed by k.
A	Set of arcs indexed by a. The arc $(i, j) \in A$ connects $i \in N$ and $j \in N$. $A_s/A_d \subseteq A$ represents the set of supply/demand arcs. For $(i, j) \in A_s/A_d$, $j \in S/D$. $A_w \subseteq A$ denotes arcs for mode w.
Parameters:	
q_o	Quantity (ton) of order o.
τ_{ij}^k	The transit time (measured in hours) for vehicle k to traverse arc (i, j).
$[a_{s(o)}, b_{s(o)}]$	The pickup time window for order o at supply points.
$[a_{d(o)}, b_{d(o)}]$	The delivery time window for order o at demand points.
$[a_i^k, b_i^k]$	The open time window for vehicle k with predefined schedules at location i.
t'^k_i	The handling time (in hours) required for vehicle k to complete loading/unloading operations at location i.
v_k	Speed (km/h) of vehicle k.
d_{ij}^k	Distance (in km) between locations i and j for vehicle k.
c_k^n	Unit cost (in CNY) of different terms, $n \in \{1, 1\prime, 2, 3, 4, 5\}$. $c_k^1/c_k^{1'}$ is the transit cost per ton per hour/km for vehicle k. c_k^2 is the loading/unloading cost per ton using vehicle k. c_k^3 is the storage cost per ton per hour using vehicle k. c_k^4 is the cost per hour of waiting time using vehicle k. c_k^5 is the delay penalty per ton per hour using vehicle k.
c'_k	Capacity (ton) of vehicle k.
M	A large enough positive number.
Variables:	
x_{ij}^k	Binary variable; 1 if vehicle k traverses arc (i, j), 0 otherwise.
y_{ij}^{ko}	Binary variable; 1 if order o carried by vehicle k traverses arc (i, j), 0 otherwise.
z_{ij}^k	Binary variable; 1 if location i is positioned prior to location j (not necessarily adjacent) in the path of vehicle k, 0 otherwise.
$s_{io}^{kk'}$	Binary variable; 1 if order o is transferred from vehicle k to vehicle $k' \neq k$ at transshipment location i, 0 otherwise.
$t_i^{ko}/t'^{ko}_i/\bar{t}_i^{ko}$	The arrival/service begin/service finish time of order o at location i served by vehicle k.
$t_i^k/t'^k_i/\bar{t}_i^k$	The arrival/service start/departure time for vehicle k at location i.
t_{ki}^{wait}	The idle duration of vehicle k at location i.
t_o^{delay}	The delay time of order o at demand location.

and applicability. There is no fixed or maximum number of delivery points that a drone must visit in a single trip. A drone may visit multiple destinations as needed to minimize cost and maximize service rate. After completing its delivery route, each drone is required to return to its original takeoff location, where it remains on standby for potential future tasks.

Following a disaster, q surrounding cities serve as supply points to support the affected area (AA), represented by the set $S = \{S_i\}_{i=1}^q$. The set $T = \{T_i\}_{i=1}^n$ represents transfer points, while the set $T' = \{T'_i\}_{i=1}^n$ denotes preset drone takeoff points–essentially a subset of T used for transitioning between modes and drone launch. The locations of T' are determined using Thiessen polygon theory (Cao and Glover, 2010) to ensure fair and complete spatial coverage in the disaster area.

Fig. 2 illustrates the coordination network for drones and multimodal transport in emergency supply delivery. This network is represented as (N, A), where N denotes the set of nodes (e.g., supply points S, transfer points T, takeoff points T', demand points D, and road disruption points B), and A denotes the set of arcs. The objective is to minimize the total cost c, which includes monetary costs (e.g., transit and transfer) and time-related costs (e.g., waiting time and delay penalties). Based on Fig. 2, we introduce four typical transport scenarios.

(a) $S_1 \rightarrow T'_1 \rightarrow D_1$: This is a dedicated route for emergency relief supplies. Supplies o_e and o_u are transported from S_1 to the drone takeoff point T'_1 via k_r and k_h. Drones (k_u) then take off from T'_1 and deliver o_e to D_1.

(b) S_2 & $S_3 \rightarrow T_2 \rightarrow B \rightarrow D_2$: Supplies o_e, o_n, and o_u are transported from S_2 and S_3 to T_2 using k_r and k_h. From T_2, k_h continues to carry the cargo. Upon reaching a disruption point B in the affected area AA, road L is found to be impassable. At B, drones transition from cargo to carrier state ($o_u \rightarrow k_u$), take off with o_e from k_h, and dynamically plan a new route L' to deliver o_e to D_2. This scenario highlights the dynamic adaptability of drone-integrated logistics–something infeasible in traditional multimodal networks.

(c) S_3 & $S_4 \rightarrow T_3 \rightarrow T'_3 \rightarrow D_3$: This route illustrates cargo heterogeneity and truck-drone coordination. Supplies o_e, o_n, and o_u are transported from S_3 and S_4 to T_3 via k_r and k_f (as T_3 accommodates aircraft k_f, unlike other transfer points). Then, k_h moves all supplies to the drone takeoff point T'_3 (located via Thiessen polygons). Drones (k_u) deliver o_e to D_3, while trucks (k_h) proceed to deliver o_n along the planned route L.

(d) $S_3 \rightarrow D_1$: When D_1 urgently requires a large volume of o_e, aircraft k_f directly airlifts o_e from S_3 to D_1 for rapid airdrop delivery.

The DMT-Drones problem features multimodal transport, transfers, complex scheduling, cargo heterogeneity, and vehicle synchronization, as illustrated in Fig. 3. To clearly illustrate the DMT-Drones problem, the real-world transport network is decomposed into four layers, each corresponding to the route planning and scheduling of a specific vehicle type: the k_r (rail), k_h (road), k_u (drone), and k_f (flight) layers. In this study, vehicle routes (k) and order assignments (o) are planned simultaneously. Each order o can be

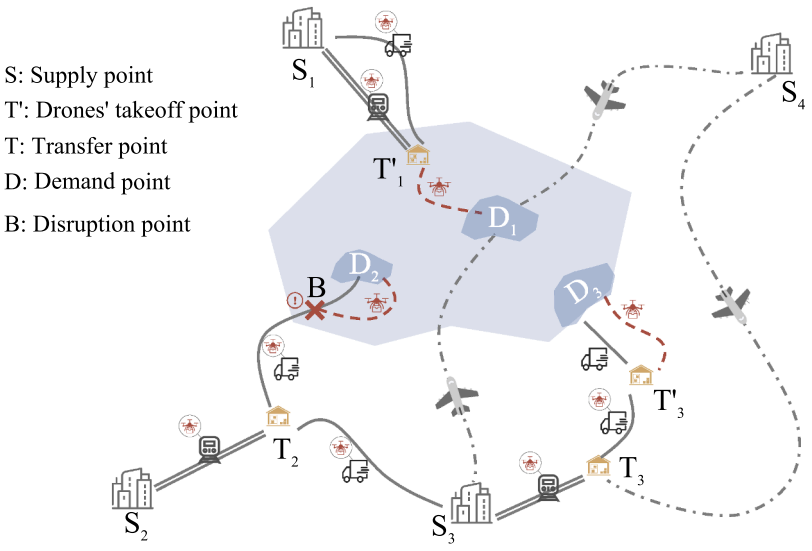

Fig. 2. A network of drone and multimodal transport coordination in emergency logistics.

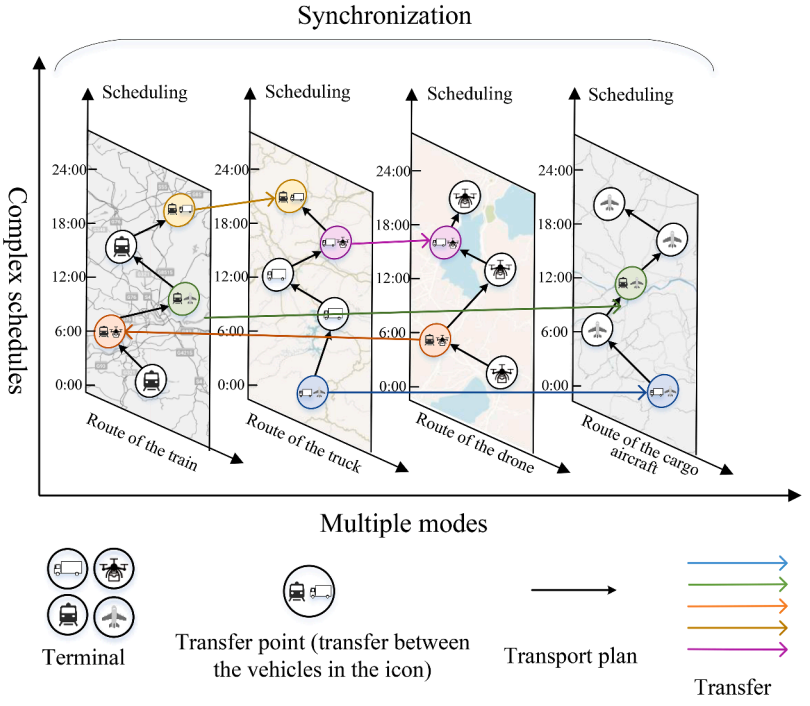

Fig. 3. Characteristics of the DMT-Drones.

transported using any combination of these four modes, depending on their distinct characteristics: k_r offers the lowest cost and highest capacity; k_h provides balanced cost, speed, and capacity; k_u offers maximum flexibility but limited capacity; and k_f is the fastest, yet most expensive and least available.

Any order o can be transferred between different vehicles k at transfer points T, which are equipped with transfer facilities and yard space for temporary cargo storage. These points also function as regular terminals, enabling them to serve as pickup or delivery locations. Transfers are not limited to different modes; they can also occur between vehicles of the same mode operating on different schedules. Flexible transport modes such as k_h and k_u greatly increase transfer opportunities. As shown in Fig. 3, this study also incorporates transfer times between modes at T.

This study incorporates scheduling considerations such as waiting time, storage time, and delivery delay. When a vehicle k arrives at a pickup point $s(o)$ or transfer point T before the order o, it must wait for o to arrive. Conversely, if o arrives before k, it incurs

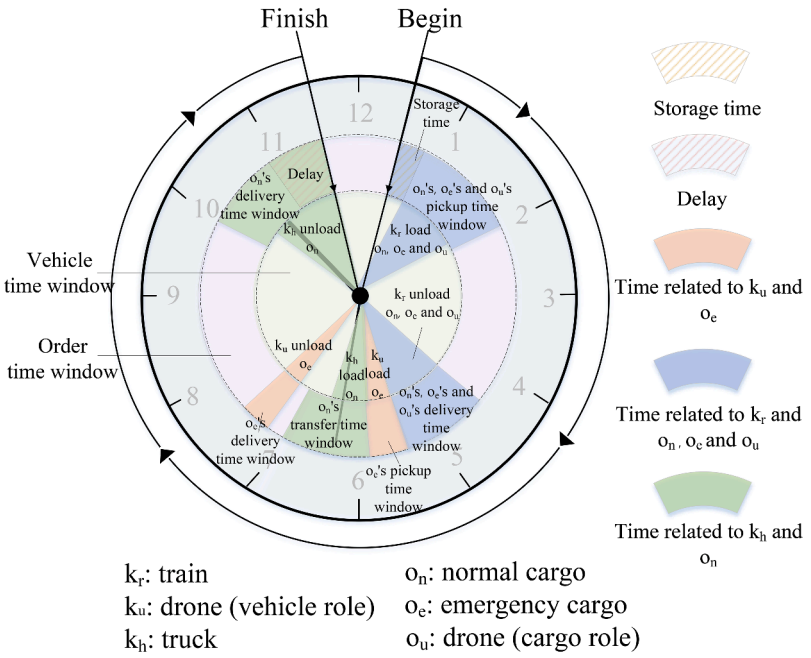

Fig. 4. Complex schedules and cargo heterogeneity.

storage time and associated fees until the vehicle arrives. Delays at the delivery terminal result in penalty costs c_k^5 for vehicles. Transfers between vehicles can affect both waiting and delay times, as one vehicle's schedule may depend on another. To maintain synchronization, waiting and storage times are dynamically adjusted. As illustrated in Fig. 4, the DMT-Drones problem involves intricate scheduling and diverse cargo characteristics.

The time window for trains (k_r) to load normal orders (o_n), emergency orders (o_e), and drone cargo units (o_u) is [1, 2], while the pickup time window is [0.5, 2]. Thus, loading is completed at time 1, and the train arrives at transfer point T at time 4.5. At T, the unloading window for k_r and the delivery window for o_e, o_n, and o_u are both [4.5, 5.5]. Immediately after unloading, order-state drones (o_u) transition to vehicle-state drones (k_u) and begin loading o_e within a time window aligned with o_e's delivery window of [5.5, 5.8]. At time 5.8, k_u takes off to deliver o_e to demand point D. Simultaneously, trucks (k_h) begin loading o_n within the window [5.8, 6.5], with o_n's pickup window being [5.8, 7]. Loading is completed at 6.5, and k_h departs for D. Drones k_u arrive at D and unload o_e at time 7.2, within its delivery window of [7.2, 7.4]. Trucks k_h arrive at D at 10.5. However, since o_n's delivery window at D is [10, 10.9] and k_h's unloading window is [10.5, 11.6], the delivery incurs a delay of 0.7 h.

The solution to the DMT-Drones problem is dynamically updated to respond to unexpected events (e.g., road damage caused by disasters), ensuring both operational efficiency and timely delivery. An initial solution X is first constructed. When disruptions occur, the solution is adjusted dynamically by rerouting vehicles, changing transport modes for affected requests, and modifying drone takeoff points T'.

A solution is defined as a set of routes $X = X_k : k \in K$, where each route X_k starts and ends at a depot. At any time t, the total weight of cargo on vehicle k must not exceed its capacity c'_k. For each order o, the pickup location $s(o)$ and delivery location $d(o)$ may be served by the same vehicle k, with $d(o)$ scheduled after $s(o)$. Alternatively, they may be served by different vehicles (e.g., k_1, $k_2 \in K$), requiring transshipment–where k_2 can begin service only after k_1 has unloaded the cargo at the transfer point. Each order o must be picked up within its time window $[a_{s(o)}, b_{s(o)}]$ and delivered within $[a_{d(o)}, b_{d(o)}]$, though late deliveries are allowed with penalties. Vehicles may wait at locations for cargo to arrive, and orders may be temporarily stored at intermediate points if vehicles have not yet reached the location.

The following assumptions are made in this study: (a) the exact timing and scope of the disaster are not predicted, but the demand in the affected area is assumed to be known; (b) time uncertainty is not modeled explicitly; however, transport disruptions such as road damage or network failure caused by disasters are considered; (c) storage capacity at transfer points is assumed to be unlimited.

4. The rolling horizon approach for dynamic planning

We address dynamic planning in the face of unexpected disruptions, such as sudden damage to roads, railways, or terminals caused by disasters. In such events, affected vehicles halt at their current locations, and the model dynamically recalculates feasible routes to maintain service continuity. If a vehicle carries cargo-state drones and no viable route is available, the drones are deployed directly from the vehicle's current position. These drones then fly to designated demand points to deliver emergency supplies and return to their original deployment site, enabling an agile and effective disaster response. Fig. 5 illustrates this dynamic adjustment process. Initially, the planned route from a supply point S to a demand point D includes a predefined drone takeoff point T_1. When an unexpected disruption occurs at point B, the original route becomes invalid. The model then generates a new takeoff point T_2,

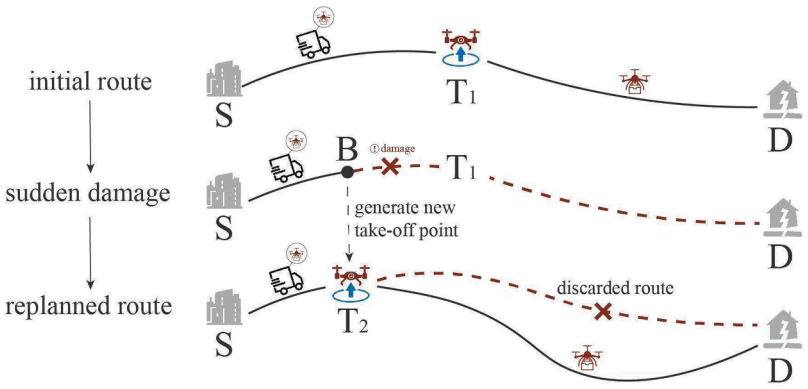

Fig. 5. Real-time changes in drone takeoff points and replanning of routes under sudden damage.

discards the damaged segment, and replans the route accordingly. This approach ensures uninterrupted supply delivery, even under rapidly changing conditions.

We employ an event-triggered rolling horizon replanning approach for dynamic planning (Anuar et al., 2022), as illustrated in Algorithm 1 and depicted in Fig. 6. We choose the rolling horizon approach for its adaptability to dynamic post-disaster environments, where conditions such as infrastructure, demand, and supply change rapidly. This method supports real-time decision updates, offers a favorable balance between solution quality and computational efficiency under time-critical constraints (Lu et al., 2016), and enables sequential re-optimization across multiple transport modes (e.g., truck, drone, helicopter, rail). Alternative methods include Model Predictive Control (MPC), which is conceptually similar to rolling horizon but grounded in control theory (Liu et al., 2019; Wan et al., 2022; Souto et al., 2024). Reinforcement Learning (RL) can learn adaptive policies under uncertainty and has been applied in logistics, but it typically requires large training datasets and significant computational resources, limiting its practicality in real-time disaster response. Stochastic programming explicitly models uncertainty through scenario-based formulations, yet it often becomes computationally intractable for large-scale or time-critical applications (Meng et al., 2023; Rodríguez-Espíndola et al., 2023). Robust optimization offers a distribution-free way to handle uncertainty but may lead to conservative decisions that reduce operational efficiency. While these methods offer potential advantages, the rolling horizon approach strikes a suitable balance between practicality and performance in context of post-disaster logistics.

We define the planning time horizon as the interval $[t_0, t_n]$. Initially, the model optimizes the path L for vehicle k within $[t_0, t_1]$ based on current information. At time $t_e \in [t_0, t_1]$, if an external event occurs (e.g., road damage due to secondary disasters), the remaining path $L_{(t_e,t_1)}$ is discarded, and re-planning is triggered for the new time horizon $[t_e, t_2]$, using real-time information about the external event. If no further events occur within $[t_e, t_2]$, the vehicle continues along the planned path. At t_2, path optimization is extended to the next interval $[t_2, t_3]$, fixing the path $L_{(t_0,t_2)}$. If an event occurs at any $t_i' \in [t_e, t_2]$, re-planning is triggered again. This rolling horizon approach iterates until the final stage t_f, completing the dynamic optimization for $[t_0, t_n]$, ensuring real-time path updates throughout the planning horizon.

Algorithm 1: Dynamic planning with drone deployment for disaster response.

```
Input: Initial routes X, vehicle locations L, terminal locations N, disaster events E, disaster demand points D;
Output: Updated routes X', which includes drone deployment plan;
while disaster events E occur do
    for affected roads, railways, or terminals in E do
        if feasible new route exists for k then
            Update route X' using ALNS algorithm;
        else
            if drones are available on vehicle k then
                Identify disaster demand points D near current location i;
                Treat current location i as new drones' takeoff point;
                Deploy drones to service demand points using the ALNS algorithm;
                Update the route X' by incorporating the drone deployment plan;
            end
        end
    end
end
Return: Updated routes X'.
```

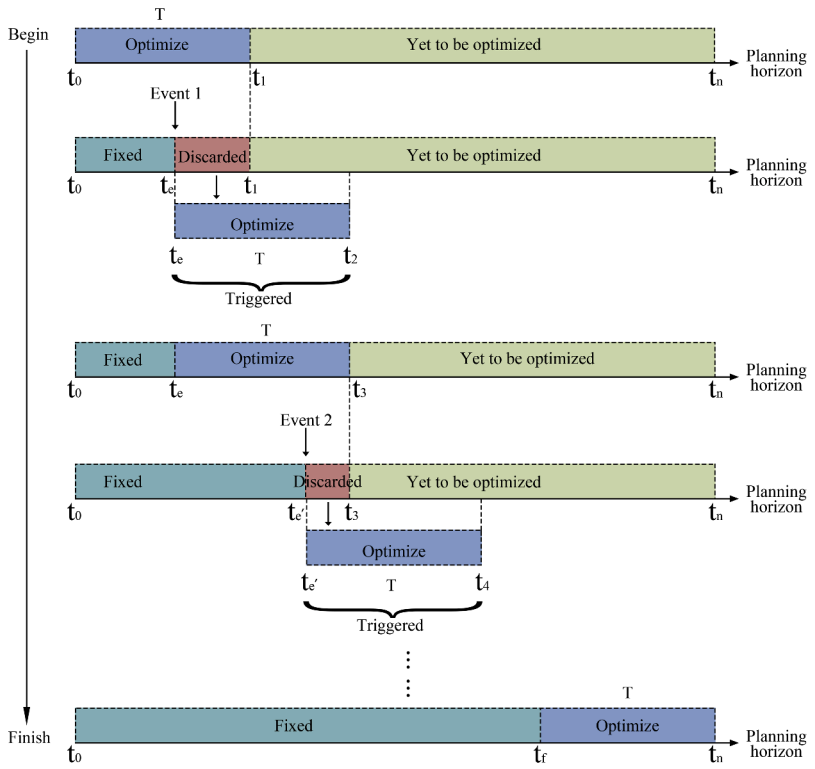

Fig. 6. Schematic illustration of event-triggered replanning using a rolling horizon approach.

5. Mathematical model

Similar to approaches in other studies (Barbarosoglu and Arda, 2004; Clark and Culkin, 2013; Haghani and Oh, 1996; Hu, 2011; Haghani, 1997; Zhu et al., 2008), the objective of the proposed DMT-Drones is to minimize the total cost (CNY), which includes transit cost (F_1), transfer cost (F_2), storage cost (F_3), waiting cost (F_4), and delay penalty (F_5), as defined in Eqs. (1)–(6).

$$\min \ F = F_1 + F_2 + F_3 + F_4 + F_5 \tag{1}$$

$$F_1 = \sum_{k\in K}\sum_{(i,j)\in A}\sum_{o\in O}(c_k^1\tau_{ij}^k + c_k^{1'}d_{ij}^k)q_o y_{ij}^{ko} \tag{2}$$

$$F_2 = \sum_{k,l\in K,k\neq l}\sum_{o\in O}\sum_{i\in T}(c_k^2 + c_l^2)q_o s_{io}^{kl} + \sum_{k\in K}\sum_{(i,j)\in A_s}\sum_{o\in O}c_k^2 q_o y_{ij}^{ko} + \sum_{k\in K}\sum_{(i,j)\in A_d}\sum_{o\in O}c_k^2 q_o y_{ij}^{ko} \tag{3}$$

$$F_3 = \sum_{k,l\in K,k\neq l}\sum_{o\in O}\sum_{i\in T}c_k^3 q_o s_{io}^{kl}(t'^{lo}_i - \bar{t}_i^{ko}) + \sum_{k\in K}\sum_{(i,j)\in A_s}\sum_{o\in O}c_k^3 q_o y_{ij}^{ko}(t'^{ko}_i - a_{s(o)}) \tag{4}$$

$$F_4 = \sum_{k\in K}\sum_{i\in N}c_k^4 t_{ki}^{\text{wait}} \tag{5}$$

$$F_5 = \sum_{o\in O}c_k^5 q_o t_o^{\text{delay}} \tag{6}$$

Constraints (7) and (8) enforce the requirement that each vehicle must start and end its route at its designated origin and destination depots, respectively. Constraints (7) and (8) do not restrict the routes of truck services, as the fleet is treated as multiple trucks, each potentially following distinct routes. The subtour elimination constraints, given by Constraints (9)–(11), establish tight bounds and are among the most compact formulations in polynomial-sized subtour elimination methods. To ensure correct order fulfillment, Constraints (12) and (13) require that cargo for every order be picked up at their specified supply location and delivered to the corresponding demand location. Finally, Constraints (14) impose capacity restrictions.

$$\sum_{j\in N}x_{\bar{o}(k)j}^k \leqslant 1 \quad \forall k \in K \setminus K_h \tag{7}$$

$$\sum_{j\in N}x_{\bar{o}(k)j}^k = \sum_{j\in N}x_{j\bar{o'}(k)}^k \quad \forall k \in K \setminus K_h \tag{8}$$

$$x_{ij}^k \leqslant z_{ij}^k \quad \forall i,j \in N,\ \forall k \in K \setminus K_h \tag{9}$$

$$z_{ij}^{k} + z_{ji}^{k} = 1 \quad \forall i, j \in N,\ \forall k \in K \setminus K_h \tag{10}$$

$$z_{ij}^{k} + z_{jp}^{k} + z_{pi}^{k} \leqslant 2 \quad \forall i, j, p \in N,\ \forall k \in K \setminus K_h \tag{11}$$

$$\sum_{k \in K} \sum_{j \in N} y_{s(o)j}^{ko} = 1 \quad \forall o \in O \tag{12}$$

$$\sum_{k \in K} \sum_{i \in N} y_{id(o)}^{ko} = 1 \quad \forall o \in O \tag{13}$$

$$\sum_{o \in O} q_o y_{ij}^{ko} \leqslant c_k' x_{ij}^{k} \quad \forall (i, j) \in A,\ \forall k \in K \tag{14}$$

Constraints (15) and (16) govern the transshipment process. Constraints (15) ensure that transshipment occurs at most once at a given location, while constraints (16) prohibit transshipment within the same vehicle k.

$$\sum_{j \in N} y_{ji}^{ko} + \sum_{j \in N} y_{ij}^{lo} \leqslant s_{io}^{kl} + 1 \quad \forall o \in O,\ \forall i \in T,\ \forall k, l \in K \tag{15}$$

$$s_{io}^{kk} = 0 \quad \forall o \in O,\ \forall i \in T,\ \forall k \in K \tag{16}$$

Flow conservation for both vehicles and orders is managed by Constraints (17)–(22). Specifically, Constraints (17) handle the conservation of vehicle flows, while Constraints (18)–(21) address order flow conservation. Constraints (18) apply to regular locations, whereas Constraints (19) govern transshipment locations. To account for scenarios where a vehicle k passes a transshipment location $i \in T$ without transferring an order, Constraints (20) and (21) ensure proper order flow conservation. This situation arises when order o is not transferred at location i, but vehicle k visits the location to handle other orders. Finally, Constraints (22) link the variables y_{ij}^{ko} and x_{ij}^{k}, ensuring that an order can be transported along an arc only if the corresponding vehicle traverses that arc.

$$\sum_{j \in N} x_{ij}^{k} - \sum_{j \in N} x_{ji}^{k} = 0 \quad \forall k \in K \setminus K_h,\ \forall i \in N \setminus \overline{o}(k), \overline{o'}(k) \tag{17}$$

$$\sum_{j \in N} y_{ij}^{ko} - \sum_{j \in N} y_{ji}^{ko} = 0 \quad \forall k \in K,\ \forall o \in O,\ \forall i \in N \setminus T, s(o), d(o) \tag{18}$$

$$\sum_{k \in K} \sum_{j \in N} y_{ij}^{ko} - \sum_{k \in K} \sum_{j \in N} y_{ji}^{ko} = 0 \quad \forall k \in K,\ \forall o \in O,\ \forall i \in T \setminus s(o), d(o) \tag{19}$$

$$\sum_{j \in N} y_{ij}^{ko} - \sum_{j \in N} y_{ji}^{ko} \leqslant \sum_{l \in K} s_{io}^{lk} \quad \forall k \in K,\ \forall o \in O,\ \forall i \in T \setminus s(o), d(o) \tag{20}$$

$$\sum_{j \in N} y_{ji}^{ko} - \sum_{j \in N} y_{ij}^{ko} \leqslant \sum_{l \in K} s_{io}^{kl} \quad \forall k \in K,\ \forall o \in O,\ \forall i \in T \setminus s(o), d(o) \tag{21}$$

$$y_{ij}^{ko} \leqslant x_{ij}^{k} \quad \forall (i, j) \in A,\ \forall k \in K,\ \forall o \in O \tag{22}$$

Constraints (23)–(25) incorporate the unique characteristics of multimodal transport. Specifically, Constraints (23) prevent vehicles from using unsuitable routes–for instance, trucks are not permitted on railway tracks. Constraints (24) address predefined routes assigned to certain vehicles, while Constraints (25) ensure that transshipment occurs at appropriate locations, as some transshipment points support transfers only between specific transport modes. For example, when cargo needs to be transferred from trains to trucks, locations designated solely for transshipment between trains and aircraft are excluded. These constraints are distinctive to this model, reflecting the specific requirements of vehicle routing in multimodal transport systems.

$$x_{ij}^{k} = 0 \quad \forall k \in K_w,\ \forall (i, j) \in A \setminus A_w,\ \forall w \in W \tag{23}$$

$$x_{ij}^{k} = 0 \quad \forall k \in K_r,\ \forall (i, j) \in A \setminus A_r^{k} \tag{24}$$

$$s_{io}^{kl} = 0 \quad \forall k \in K_{w_1},\ \forall l \in K_{w_2},\ \forall i \in T \setminus T_{w_1}^{w_2},\ \forall o \in O,\ \forall w_1, w_2 \in W \tag{25}$$

Constraints (26)–(30) impose time-related restrictions on services, including loading, unloading, and transshipment. Constraints (26) ensure that the service start time occurs after the arrival of the cargo. Constraints (27) define the service finish time as the sum of the service start time and the duration of the service. Constraints (28) require that departures take place only after all services have been completed. Constraints (29) stipulate that an order's arrival time cannot precede the arrival time of the vehicle. Lastly, Constraints (30) specify the latest allowable start time for a vehicle's final service.

$$t_i^{ko} \leqslant t'^{ko}_i \quad \forall i \in N,\ \forall k \in K,\ \forall o \in O \tag{26}$$

$$t'^{ko}_i + t''^{ko}_i \sum_{j \in N} y_{ij}^{ko} \leqslant \bar{t}_i^{ko} \quad \forall i \in N,\ \forall k \in K \setminus K_h,\ \forall o \in O \tag{27}$$

$$\bar{t}_i^{k} \geqslant \bar{t}_i^{ko} \quad \forall i \in N,\ \forall k \in K \setminus K_h,\ \forall o \in O \tag{28}$$

$$t_i^{k} \leqslant t_i^{ko} \quad \forall i \in N,\ \forall k \in K \setminus K_h,\ \forall o \in O \tag{29}$$

$$t'^{k}_i \geqslant t'^{ko}_i \quad \forall i \in N,\ \forall k \in K \setminus K_h,\ \forall o \in O \tag{30}$$

Constraints (31) and (32) guarantee the alignment between travel time, distance, and speed. Without considering waiting time, Constraints (31) alone would suffice to determine arrival time t_j^{k}. However, since this study accounts for vehicle waiting periods,

Constraints (32) are introduced to enforce strict travel time limits. Meanwhile, Constraints (33) and (34) manage time windows for supply locations and predefined locations, respectively.

$$\bar{t}_i^k + \tau_{ij}^k - t_j^k \leqslant M(1 - x_{ij}^k) \quad \forall (i,j) \in A,\ \forall k \in K \setminus K_h \tag{31}$$

$$\bar{t}_i^k + \tau_{ij}^k - t_j^k \geqslant -M(1 - x_{ij}^k) \quad \forall (i,j) \in A,\ \forall k \in K \setminus K_h \tag{32}$$

$$t'^{ko}_{s(o)} \geqslant a_{s(o)} y_{ij}^{ko},\ \bar{t}^{ko}_{s(o)} \leqslant b_{s(o)}(y_{ij}^{ko} + M(1 - y_{ij}^{ko})) \quad \forall (i,j) \in A, \forall o \in O,\ \forall k \in K \tag{33}$$

$$t_i^{ko} \geqslant a_i^k y_{ij}^{ko},\ \bar{t}_i^{ko} \leqslant b_i^k (y_{ij}^{ko} + M(1 - y_{ij}^{ko})) \quad \forall (i,j) \in A,\ \forall o \in O,\ \forall k \in K_r \tag{34}$$

Constraints (35) manage the timing of transshipment operations. In cases where cargo is transferred from vehicle k to vehicle l, and vehicle l arrives before vehicle k completes unloading, vehicle l is allowed to wait until unloading is finished. Constraints (36) and (37) calculate the waiting time and delay time, respectively, aiming to minimize both waiting periods and associated delay costs. Additionally, Constraints (38) account for the arrival times of trucks, ensuring accurate time management within the model.

$$\bar{t}_i^{ko} - t'^{lo}_i \leqslant M(1 - s_{io}^{kl}) \quad \forall o \in O,\ \forall i \in T,\ \forall k,l \in K,\ k \neq l \tag{35}$$

$$t_{ki}^{\text{wait}} \geqslant t'^k_i - t_i^k \quad \forall i \in N,\ \forall k \in K \setminus K_h \tag{36}$$

$$t_o^{\text{delay}} \geqslant (\bar{t}_{d(o)}^{ko} - b_{d(o)}) \sum_{i \in N} y_{id(o)}^{ko} \quad \forall o \in O,\ \forall k \in K \tag{37}$$

$$(t_j^{ko} - \bar{t}_i^{ko}) y_{ij}^{ko} = \tau'^{ko}_{ij} \quad \forall (i,j) \in A,\ \forall k \in K_h,\ \forall o \in O \tag{38}$$

6. Adaptive large neighborhood search

The ALNS algorithm is particularly well-suited for solving the DMT-Drones problem due to its flexibility, efficiency, and strong performance in complex, combinatorial optimization scenarios. Originally introduced by Ropke and Pisinger (2006), ALNS has since evolved into an adaptive metaheuristic framework. It iteratively applies a combination of removal and insertion operators–such as greedy, random, and regret-based strategies–to balance exploration and exploitation of the solution space. A key advantage of ALNS is its adaptability: it dynamically selects operators based on their past performance, making it highly effective across diverse problem instances.

ALNS has been successfully applied to related problems, including the Pickup and Delivery Problem with Transfers (PDPT) (Qu and Bard, 2012; Masson et al., 2013) and intermodal transport planning (Zhang et al., 2022a,b). These studies demonstrate that exact solvers like Gurobi become computationally infeasible for large-scale instances, often failing to deliver timely solutions. In contrast, ALNS consistently produces high-quality results within reasonable runtimes, even for large and complex multimodal networks (Zhang et al., 2022a). Given its effectiveness and scalability, this study adopts ALNS as the solution approach for the DMT-Drones problem.

6.1. ALNS algorithm for DMT-drones

Algorithm 2 integrates ALNS with modifications to address the specific requirements of DMT-Drones. The input (lines 1) includes a fleet of vehicles (K) such as trucks and drones, orders (O), nodes (N) representing locations (e.g., depots, transshipment points, and demand points), arcs (A) reflecting multimodal routes, and the current solution (X_{current}). The preprocessing step (line 3) ensures compatibility with multimodal and drone-specific constraints, such as restricted routes for drones or transshipment limitations between transport modes. The algorithm iteratively applies removal and insertion operators (lines 9–11) to adjust routes and schedules, dynamically balancing exploration and exploitation using a simulated annealing-based update mechanism (lines 12–16). Key modifications include ensuring drones are assigned to shorter, high-priority routes and enforcing feasibility at transshipment points for multimodal transfers. The output (line 2) is an optimized multimodal transport plan (X_{best}) that minimizes delays and costs, crucial for time-sensitive emergency logistics scenarios.

Fig. 7 illustrates the optimization process of the ALNS algorithm tailored to the DMT-Drones problem. In Fig. 7(a), the initial solution s contains multiple route intersections and overlaps across different transport modes, with relatively long and inefficient paths. Fig. 7(b) shows the intermediate solution after applying a removal operator, which eliminates selected orders by removing suboptimal or infeasible paths. Fig. 7(c) presents the refined solution after applying an insertion operator, where previously unserved demand and supply points are reassigned, reducing overlaps and significantly shortening the overall route lengths. If the resulting solution s' is worse than the current best solution s_{best}, it is discarded. The ALNS algorithm then continues iterating until the best feasible solution is identified.

6.2. Operators in ALNS for DMT-drones

To address the unique challenges of DMT-Drones, this study customizes ALNS insertion and removal operators. Removal operators destroy part of the current solution by selectively eliminating orders, while insertion operators reconstruct the solution by reintegrating the removed orders using specific heuristics. These operators consider the interdependence of drones, trucks, and trains, ensuring effective transshipments, capacity management, and prioritization of high-urgency orders. Operators are designed to balance exploration and exploitation, leveraging historical data and predictive heuristics to enhance solution quality.

Algorithm 2: ALNS for DMT-Drones.

Input: $K, O, N, A, X_{\text{current}}$; // Vehicles, orders, nodes, arcs, and current solution.
Output: X_{best} ; // Optimal multimodal transport plan.
Preprocess inputs: $[K, O, N, A] \leftarrow Preprocessing(K, O, N, A)$;
Initialize R_{pool} (unserved orders), X_{initial}, $T_{\text{Temp}} > 0$;
Set $X_{\text{last}} \leftarrow X_{\text{initial}}$, $X_{\text{best}} \leftarrow X_{\text{last}}$;
repeat
  Refresh weights and select operators based on performance;
  $[X_{\text{current}}, R_{\text{pool}}] \leftarrow RemovalOperator(X_{\text{last}}, R_{\text{pool}})$;
  while $R_{pool} \neq \emptyset$ **do**
    $[X_{\text{current}}, R_{\text{pool}}] \leftarrow InsertionOperator(X_{\text{current}}, R_{\text{pool}})$;
  end
  Update X_{last} using simulated annealing:

$$X_{\text{last}} \leftarrow \begin{cases} X_{\text{current}}, & \text{if } F(X_{\text{current}}) < F(X_{\text{last}}) \\ X_{\text{current}} \text{ with } p = e^{-\frac{F(X_{\text{current}}) - F(X_{\text{last}})}{T_{\text{Temp}}}}, & \text{otherwise.} \end{cases}$$

  if $F(X_{last}) < F(X_{best})$ **then**
    $X_{\text{best}} \leftarrow X_{\text{last}}$;
  end
  $T_{\text{Temp}} \leftarrow T_{\text{Temp}} \cdot c$; // Cooling rate c.
until *termination condition met*;

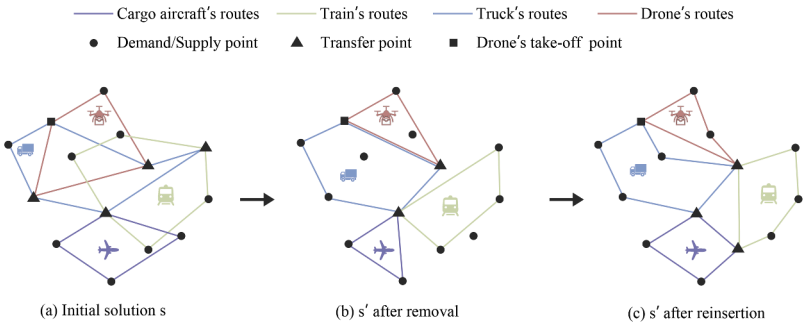

Fig. 7. Illustration of removal and insertion operations in ALNS for DMT-Drones.

6.2.1. Insertion operators

Fig. 8 presents the insertion operators employed in this study, each designed to balance efficiency and flexibility: Greedy Insertion prioritizes the lowest-cost option, Random Insertion adds stochasticity, Transshipment Insertion enables intermediate routing, Most Constrained First Insertion targets critical tasks early, and Regret Insertion considers opportunity cost. These operators are described in detail below.

Greedy insertion (Zhang et al., 2022a). This operator reconstructs a partial solution by iteratively inserting the removed orders back into the solution at the position that causes the least increase in cost. As shown in Fig. 8(a), the original route L contains orders o_1, o_2, o_3, o_4. The task requires inserting three new orders o_5, o_6, o_7 using a greedy insertion operator that evaluates all possible insertion positions for each order. Specifically, for each new order o_i, the algorithm first calculates the cost change $\Delta F_{i,p}$ for every feasible insertion position p in route L ($\Delta F_{i,p} = F_{\text{after}} - F_{\text{original}}$). Subsequently, the minimum cost $\Delta F_{i,\min}$ for each order o_i is determined by identifying the optimal insertion position p^* ($\Delta F_{i,\min} = \Delta F_{i,p^*} = \min_p\{\Delta F_{i,p}\}$). Finally, the operator selects the order-position pair that yields the smallest cost across all new orders (optimal solution $= \arg\min_{i\in\{5,6,7\}}\{\Delta F_{i,\min}\}$). This operator is essential for scenarios where drones must handle critical, time-sensitive deliveries in the multimodal network.

Random insertion (Wolfinger, 2021). As shown in Fig. 8(b), the original route L contains orders o_1, o_2, o_3. The random insertion operator introduces diversity by first uniformly selecting an order o_i from unserved orders $\{o_4, o_5, o_6\}$, then randomly choosing a feasible insertion position p along L where constraints are satisfied. This dual-random process ensures both order and position selections are stochastic, promoting global exploration to escape local optima ($(o_i, p) \sim \text{Uniform}\big(\{(o, p) \mid o \in \{o_4, o_5, o_6\}, p \in P_o\}\big)$, where P_o represents valid positions for inserting o without violating constraints).

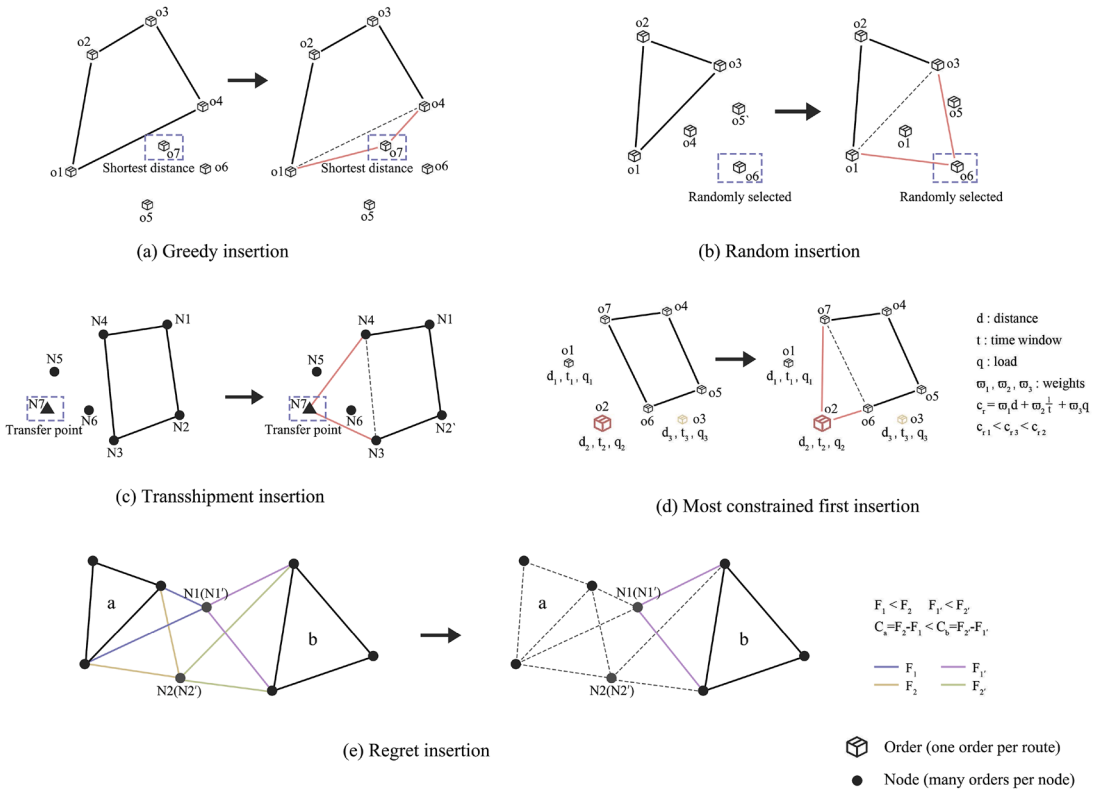

(a) Greedy insertion (b) Random insertion

(c) Transshipment insertion (d) Most constrained first insertion

(e) Regret insertion

Fig. 8. Insertion operators.

Transshipment insertion. This operator employs a greedy insertion strategy to build routes, but uniquely restricts its search to solutions that involve transshipment points and require multi-vehicle cooperation. Specifically, it prioritizes inserting requests at transshipment nodes (e.g., drone launch sites) to create hybrid delivery modes (e.g., truck-to-drone transfers). As illustrated in Fig. 8(c), given a route $L = \{N_1, N_2, N_3, N_4\}$ and candidate nodes N_5, N_6, N_7 (where N_7 is a transshipment point), the operator evaluates only the insertion of N_7 into L, generating L'. Non-transshipment nodes (e.g., N_5, N_6) are ignored unless no feasible transshipment-based insertion exists. This design increases the likelihood of forming cost-effective multi-vehicle solutions by forcing the system to first explore opportunities where drones or other vehicles are deployed from transshipment points, even if non-transshipment insertions might appear locally optimal.

Most constrained first insertion. As shown in Fig. 8(d), the original route L consists of a sequence of orders o_4, o_5, o_6, o_7. The task at hand is to insert three new orders o_1, o_2, o_3 into this route. Specifically, orders o_1, o_2, and o_3 have transportation distances d_1, d_2, d_3; time windows t_1, t_2, t_3; and loads q_1, q_2, q_3, respectively. The time window t is calculated as $t = |b_{p(o)} - a_{p(o)}| + |b_{d(o)} - a_{d(o)}|$, which represents the sum of the widths of the pickup and delivery time windows. Most Constrained First Insertion operator assigns reasonable weights $\varpi_1, \varpi_2, \varpi_3$ to d, t, q respectively, and calculates the priority of each order through weighted averaging. The priority calculation for order o is as follows:

$$C_r = \varpi_1 d_o + \varpi_2 \left(\frac{1}{|b_{p(o)} - a_{p(o)}| + |b_{d(o)} - a_{d(o)}|} \right) + \varpi_3 q_o \tag{39}$$

According to this equation, it is clear that orders with longer transportation distances, shorter pickup and delivery time windows (i.e., higher urgency), and larger loads have higher priorities. In the example shown in Fig. 8(d), since $C_{r_1} < C_{r_3} < C_{r_2}$, order o_2 has the highest priority and should be transported first. Due to its effectiveness in managing orders with tight delivery time windows and significant load requirements, especially in scenarios involving urgent deliveries by drones, this operator is highly suitable for addressing the DMT-Drones problem.

Regret insertion (Ropke and Pisinger, 2006). The Regret Insertion operator selects the order based on the largest regret value between the best and second-best insertion costs, aiming to prioritize difficult-to-place orders early. This operator is valuable in emergency logistics, as it helps prioritize orders that may become more costly or infeasible in future iterations. As shown in Fig. 8(e), two nodes are to be inserted into paths a and b, denoted as N_1, N_2 for a, and N_1', N_2' for b. The optimal insertion strategy is determined as follows:

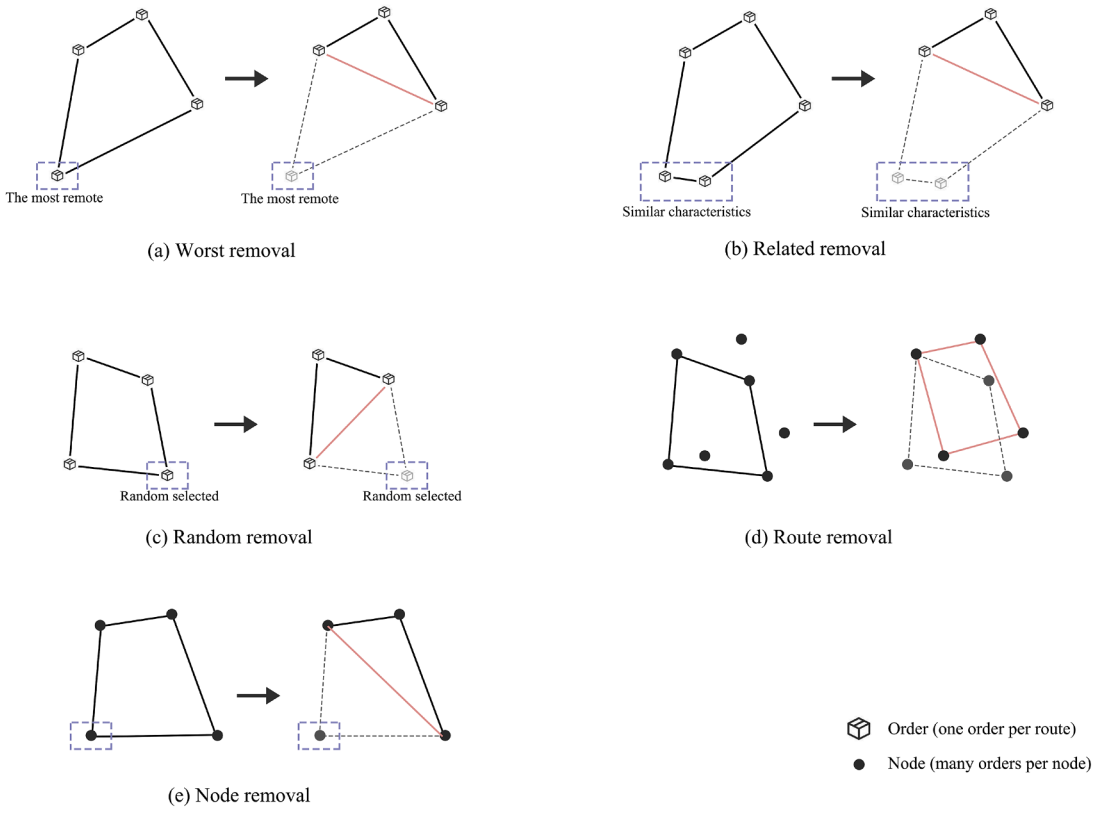

Fig. 9. Removal operators.

(a) Insert N_1 and N_2 into path a, compute insertion costs ΔF_1, ΔF_2, and define the best insertion cost $\Delta F_{\text{best},a} = \min(\Delta F_1, \Delta F_2)$ and $\Delta F_{\text{second},a}$ as the other. In the figure, $\Delta F_{\text{best},a} = \Delta F_1$, $\Delta F_{\text{second},a} = \Delta F_2$.
(b) Similarly, insert N_1', N_2' into path b, yielding costs $\Delta F_1'$, $\Delta F_2'$, with $\Delta F_{\text{best},b} = \min(\Delta F_1', \Delta F_2')$ and $\Delta F_{\text{second},b}$ as the other.
(c) The regret insertion operator estimates the future cost impact using the regret value ($c_a = \Delta F_{\text{second},a} - \Delta F_{\text{best},a}$, $c_b = \Delta F_{\text{second},b} - \Delta F_{\text{best},b}$).
(d) Compare c_a and c_b; the path with higher regret is selected. In this case, $c_a < c_b$, so path b is chosen, and N_1' (with lower cost) is inserted.

6.2.2. Removal operators

We employ five removal operators (Worst Removal, Related Removal, Random Removal, Route Removal, and Node Removal), each of which targets solution diversification from a different perspective, as shown in Fig. 9. The following provides detailed illustrations of these operators.

Worst removal (Ghilas et al., 2016). Worst Removal operator removes the order o_i with the highest cost, as shown in Fig. 9(a). To diversify the search, a noise factor within $[1-\delta, 1+\delta]$ ($\delta < 1$) is applied to distance components in the cost calculation (Cunha et al., 2024). This is crucial for multimodal transportation where drones handle high-cost last-mile deliveries, as reallocating these orders can reduce overall costs.

Related removal (Ropke and Pisinger, 2006). As shown in Fig. 9(b), related removal operator removes clusters of similar orders based on distance, time, load, and vehicle compatibility. For example, orders served by drones within a certain geographic radius may be removed together to evaluate alternative routing strategies. For the DMT-drones, we define the relatedness r_{ij} between two orders i and j based on the distance (Ropke and Pisinger, 2006). Since each order o_i encompasses a pickup node i/j and a delivery node $i+n/j+n$, we derive the following equation (Pisinger and Ropke, 2007):

$$r_{ij} = \frac{1}{D}(d(i,j) + d(i,j+n) + d(i+n,j) + d(i+n,j+n)) \tag{40}$$

The denominator D counts the number of pickups and deliveries not occurring at the same terminal, ranging from 1 to 4 depending on their locations.

Random removal (Danloup et al., 2018). As shown in Fig. 9(c), the Random Removal operator randomly selects and removes one of the orders o_i. This operator promotes solution diversity by preventing drones and other vehicles from being limited to fixed or repetitive routing patterns.

Route removal. As shown in Fig. 9(d), The Route Removal operator clears route L by removing all passed nodes N, returning them and their associated orders o_i to the order pool for potential reconstruction into improved routes. This is especially beneficial in multimodal scenarios, where consolidating routes helps reduce vehicle usage and enhance drone efficiency. (Majidi et al., 2018).

Node removal. As shown in Fig. 9(e), node removal operator removes a specific node N_i from route L. For example, removing a truck terminal may result in reallocating orders to drones for direct delivery, reducing overall transit time.

6.3. Feasibility checking and synchronization

Feasibility checks and synchronization are critical to ensuring that the multimodal solution complies with all operational constraints. Each insertion updates vehicle schedules, coordinates interactions between different vehicles (e.g., drones and trucks at transshipment points), and verifies feasibility with respect to capacity limits, time windows, and intermodal compatibility.

Transfers can create cascading effects, where a change in one vehicle's route impacts others and potentially disrupts the entire plan. Synchronization is therefore crucial to coordinate vehicles across modes and minimize deviations from the intended schedule. The complexity of transfer systems adds to the challenge of temporal alignment. For example, order o_1 may be handled by cargo aircraft, trains, and trucks, requiring two transfers–first from aircraft to train, then from train to truck. Introducing a new order o_2 into the aircraft's route alters its schedule, which in turn affects the truck's plan due to the interdependency created by o_1. Similarly, train schedule changes caused by handling both o_1 and o_2 at a transfer terminal may ripple back to disrupt the aircraft and truck timelines. Effective synchronization ensures that delays in one mode (e.g., trains) do not propagate to others (e.g., drones), enabling the system to adapt dynamically to emergency logistics scenarios and maintain timely, efficient deliveries.

7. Numerical experiments

This section presents the numerical experiments conducted to evaluate the performance and effectiveness of the proposed DMT-Drones model and solution approach. The ALNS algorithm is configured with a cooling rate of 0.9 and operator weights updated every 20 iterations. The computation time for each instance is capped at 72 h. The algorithm is implemented in Python 3.10 and executed on a Windows 11 system with 16 GB RAM and an AMD Ryzen 7 5800H processor running at 3.20 GHz.

This study focuses on the Luding earthquake that struck Sichuan Province, China, on September 5, 2022, resulting in 93 fatalities, 424 injuries, and 24 missing persons (Wikipedia, 2024). As shown in Fig. 10, the logistics network includes 8 supply points (S), 23 demand points (D), and 5 transfer points (T). Preset drone takeoff points (T') are determined using Thiessen polygon theory to ensure equitable and comprehensive coverage of the disaster area (Cao and Glover, 2010). The process involves: (a) dividing the region based on geographic features, demand locations, and transport accessibility; (b) generating Thiessen polygons centered on demand points to ensure that each location is closest to a designated center; and (c) selecting optimal takeoff points within each polygon based on drone range, endurance, and delivery efficiency. Optimization techniques, including shortest path and coverage algorithms, are applied to refine both the location and number of takeoff points for improved logistics performance. In this experiment, 4 preset drone takeoff points are established prior to deployment, with flexibility to adjust their locations and quantities dynamically in response to evolving emergency conditions.

Fig. 11 presents the transport network linking major cities in Sichuan Province, encompassing railway lines, highways, and air routes. All relief supplies are delivered through this network. For long-distance transport from supply points (S) to transfer points (T) or preset drone takeoff points (T'), the system utilizes trucks (k_h), trains (k_r), and cargo aircraft (k_f). For last-mile distribution from T or T' to disaster sites (D), trucks (k_h) and drones (k_u) are primarily employed. A summary of transport costs, loading/unloading fees, storage costs, waiting time charges for each vehicle type is provided in Table A.1. All datasets are publicly accessible in an online repository [1].

The first 72 h following a disaster are critical for survival without access to food or water. As noted by Huang et al. (2011) and Hakami et al. (2013), the survival rate is approximately 90 % within the first 24 h, drops to 50–60 % between 25 and 48 h, and further declines to 20–30 % between 49 and 72 h–falling below 10 % thereafter. To simulate the probability of new emergency orders over time, this study adopts the skew-normal distribution, following Azzalini and Capitanio (1999) and Sumalee et al. (2013), due to its effectiveness in modeling skewed and time-sensitive demand patterns. The probability density function of the skew-normal distribution is given by:

$$f(x) = 2\phi\left(\frac{x-\xi}{\omega}\right)\Phi\left(\alpha\left(\frac{x-\xi}{\omega}\right)\right) \tag{41}$$

where $\phi(z)$ and $\Phi(z)$ denote the probability density function and cumulative distribution function of the standard normal distribution, respectively. The parameters are defined as follows: ξ is the position parameter ($\xi = 10$), ω is the scale parameter ($\omega = 20$), and α is the shape parameter ($\alpha = 7$). As shown in Fig. 12, these parameter values effectively model the generation of new orders within the 72-h post-earthquake period. Notably, 94.27 % of orders are generated between 5 and 48 h, aligning well with real-world demand.

[1] https://github.com/ShuyangZhu/DMT-Drones_original_data

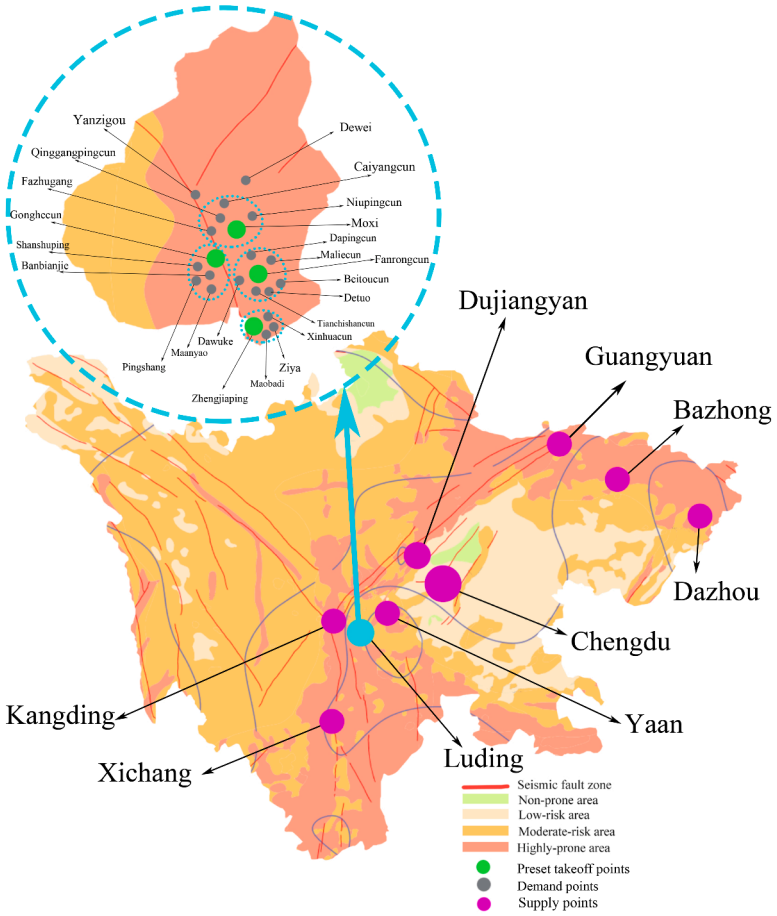

Fig. 10. The location of supply, demand, and preset takeoff points.

Fig. 11. Transport network between supply (transfer) points.

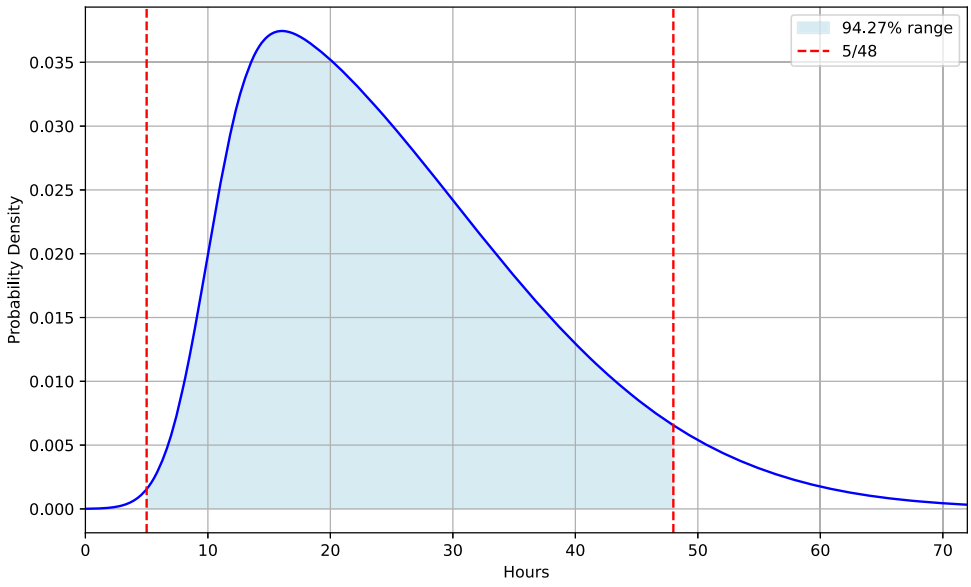

Fig. 12. Probability density of newly generated orders.

Table 3
Comparison with commercial solvers.

Problem scale			Total cost (CNY)		Gap	Best time (s)		Ratio
$\|O\|$	Variable	Constraint	Exact approach	ALNS	(%)	Exact approach	ALNS	(%)
1	13,935	35,822	1813.21	1813.21	0	48.92	0.02	0.04
2	17,950	43,364	3626.42	3626.42	0	94.01	0.06	0.06
3	27,278	71,487	4146.33	4146.69	0.009	10800.79	0.20	0.002
5	34,869	85,584	2993.32	2993.51	0.006	23048.57	1.25	0.005
10	70,352	191,489	22510.90	22510.90	0	26584.47	2.26	0.008
20	175,446	452,226	–	13179.94	–	28,800*	2.47	–
30	247,539	619,426	–	42977.89	–	28,800*	27.12	–

$|O|$: number of orders.
∗ time limit reached (8 h). – no feasible solution has been found given the time constraint.

Table 4
Comparative analysis with Shi et al. (2024)'s model.

		Total cost (CNY)			Computation time (s)		
$\|O\|$	$\|K\|$	Proposed Approach	Benchmark Shi et al. (2024)	Gap (%)	Proposed Approach	Benchmark Shi et al. (2024)	Ratio (%)
5	3	12,813	12,813	0.0	0.01	0.42	2.4
10	5	45,301	44,364	2.1	0.21	3.77	5.6
15	7	43,476	44,837	−3.0	1.01	6.22	16.2
20	10	75,073	76,140	−1.4	1.64	8.80	18.6
25	12	65,946	68,023	−3.1	1.75	13.81	24.2
30	15	83,212	89,551	−7.1	2.44	17.48	14.0
35	18	98,486	107,741	−8.6	2.31	21.61	10.7
40	21	110,807	120,820	−8.3	4.56	22.28	20.5

$|O|$: number of orders.

7.1. Comparison with the exact approach and benchmark method

Section 7.1.1 compare our algorithm with an exact approach (Gurobi). In Section 7.1.2, we compare our model with that of Shi et al. (2024).

7.1.1. Comparison with the exact approach

Since the exact method (using Gurobi) cannot handle the full-scale network shown in Fig. 11, we use a simplified network consisting of 2 supply points, 3 transfer points, 7 demand points, and 60 vehicles to compare the performance of the exact approach and ALNS. The computation time for both methods is capped at 8 h (28,800 s). For seven instance sizes ranging from 1 to 30 orders, Table 3 summarizes the numbers of decision variables and constraints, as well as the optimal solutions and computation times for both approaches. For instances with 5 or more orders, the proportions of emergency supplies (o_e) and normal supplies (o_n) are set to 20 % and 80 %, respectively. To ensure result reliability, each instance is tested three times, and average costs and computation time are reported.

In the 1-order and 10-order instances, both approaches yield identical optimal solutions. For the 3-order and 5-order instances, ALNS's best solutions are only 0.009 % and 0.006 % higher than Gurobi's, while requiring just 0.002 %–0.06 % of Gurobi's computation time. Moreover, Gurobi fails to solve instances beyond 10 orders within the time limit, while ALNS consistently finds optimal solutions–solving even the 30-order instance in under 30 s. These results clearly demonstrate the computational efficiency and scalability of ALNS over the exact approach, as shown in Table 3.

7.1.2. Comparison with benchmark method

The most comparable study in the literature is Shi et al. (2024). Therefore, we adopt it as our benchmark and conduct experiments against it. We reproduce their model, using the same set of swap and insertion operators at each stage, vehicle dispatching rules, and all constraints. Both models are tested under identical parameter settings. Due to the limited scalability of Shi et al. (2024)'s model, the comparative experiments are conducted on seven small- to medium-scale instances with order quantities ranging from 5 to 40. The results for total cost, computation time, and their differences are summarized in Table 4.

As shown in Table 4, Shi et al. (2024)'s model yields high-quality solutions for small-scale instances (5 and 10 orders). In the 5-order instance, both models achieve the optimal solution, while in the 10-order instance, its solution cost is 2.1 % lower than that of the ALNS model. However, when the order scale exceeds 10, its performance lags behind the ALNS model, particularly for medium-scale instances (more than 30 orders), where the average solution cost is approximately 8 % higher. This performance gap may stem from the reliance of Shi et al. (2024)'s approach on primarily greedy and classical swap operators, with only a single random operator introduced in the first stage, increasing the risk of entrapment in local optima. Furthermore, in its first stage, only helicopter and truck routes are planned, with drones scheduled in the second stage, a sequencing strategy that further heightens the likelihood of local

Table 5
Impact of different operator designs on ALNS performance.

	Unit total cost (CNY/t/km)				Unit delay penalty (CNY/t/km)				Service rate (%)				Computation time (s)			
$\|O\|$	All	No-G	No-R	No-M	All	No-G	No-R	No-M	All	No-G	No-R	No-M	All	No-G	No-R	No-M
5	**1.756***	1.829	1.829	1.829	**0.277***	0.332	**0.277***	**0.277***	100	100	100	100	1.3	14.9	1.4	1.4
10	**1.327***	**1.327***	1.453	1.449	**0.147***	0.152	0.152	**0.147***	100	100	100	100	5.5	324.7	6.0	52.4
20	**1.332***	1.367	1.367	**1.332***	**0.107***	**0.107***	0.122	0.122	100	100	100	100	99.0	24.6	24.3	101.6
30	**1.634***	1.664	1.790	1.680	**0.083***	0.139	0.130	0.128	100	100	87	100	945.7	764.3	113.6	777.4
50	**1.656***	1.659	1.661	1.659	**0.255***	0.257	0.257	0.257	100	100	100	100	5134.4	175.2	105.5	2933.2

$|O|$: number of orders; All: using all operators; No-G: after removing all greedy-related removal and insertion operators; No-R: after removing all random removal and insertion operators; No-M: after removing operators specifically designed for multimodal transport (e.g., transshipment insertion operator, route removal operator, node removal operator).
$*$: The best solution.

search entrapment. In contrast, our approach employs a customized set of operators encompassing greedy, stochastic, regret-based, and multimodal transport–specific designs.

In terms of computation time, Shi et al. (2024)'s model exhibits a clear disadvantage, likely due to its two-stage design in which truck and helicopter routes are each planned twice, increasing computational complexity. By contrast, the proposed approach requires only 2.4–24.2 % of the computation time, while maintaining comparable solution quality. These results highlight the substantial computational efficiency advantage of our approach.

7.2. ALNS algorithm's performance

Section 7.2.1 examines the impact of different operator designs, Section 7.2.2 analyzes the convergence of ALNS, and Section 7.2.3 discusses the stability of ALNS by testing the algorithm in 10 repeated runs.

7.2.1. The impact of different operator designs

In this study, five insertion operators and five removal operators are employed within the ALNS framework. To investigate the impact of different operator designs on algorithm performance and solution quality, we conduct four comparative experiments with varying operator configurations: (a) All: the full set of ten operators is used; (b) No-G: greedy operators are removed, specifically the Greedy Insertion and Worst Removal operators; (c) No-R: random operators are excluded, namely the Random Insertion and Random Removal operators; (d) No-M: multimodal-specific operators are removed, including Transshipment Insertion, Most Constrained First Insertion, Route Removal, and Node Removal.

These four configurations are tested across five instance sizes, with the number of orders set to 5, 10, 20, 30, and 50, respectively. For each instance, we record the total cost, delay penalty, order service rate, and computation time. The results in Table 5 show that across all instance sizes, the All configuration, which contains the full set of operators, consistently achieves the lowest unit cost and unit delay penalty. In contrast, the other three configurations (No-G, No-R, and No-M) exhibit varying performance across instances, without a clear or consistent advantage. These findings suggest that a well-balanced combination of greedy operators, random operators, and multimodal-specific operators contributes to superior solution quality.

7.2.2. Convergence of ALNS

We evaluate the convergence of the ALNS heuristic using instances with varying numbers of orders. Fig. 13 shows the costs and number of served orders of the best solution over 200 iterations. The cost could increase when there are more served orders and the cost is minimized when the number of served orders is stable. As shown in the figure, ALNS consistently converges before termination across all instances. For small instances, convergence occurs rapidly within the early iterations, whereas for large instances, no further improvements are observed after the first 60 iterations.

7.2.3. Stability analysis of ALNS

Regarding the stability analysis of ALNS, we test all 8 instances with order sizes ranging from 5 to 400, running each instance 10 consecutive times under identical experimental conditions. The results are summarized in Table 6. We report the average value, standard deviation, and coefficient of variation across the 10 runs. For small-scale instances (order sizes of 5, 10, and 20), ALNS consistently finds the optimal solution with a coefficient of variation equal to zero. For medium- and large-scale instances (order sizes of 30, 50, 100, 200, and 400), the coefficient of variation remains below 1 %. These results demonstrate the strong stability of the proposed model.

7.3. Comparison of approaches with and without drones

By removing all cargo-state and vehicle-state drones from the original DMT-Drones model, we obtain an approach without drones. A comparative analysis is then conducted between the approaches with and without drones across three key dimensions: unit cost, transport mode share, and service rate. In this experiment, the proportions of emergency supplies (o_e) and normal supplies (o_n) are

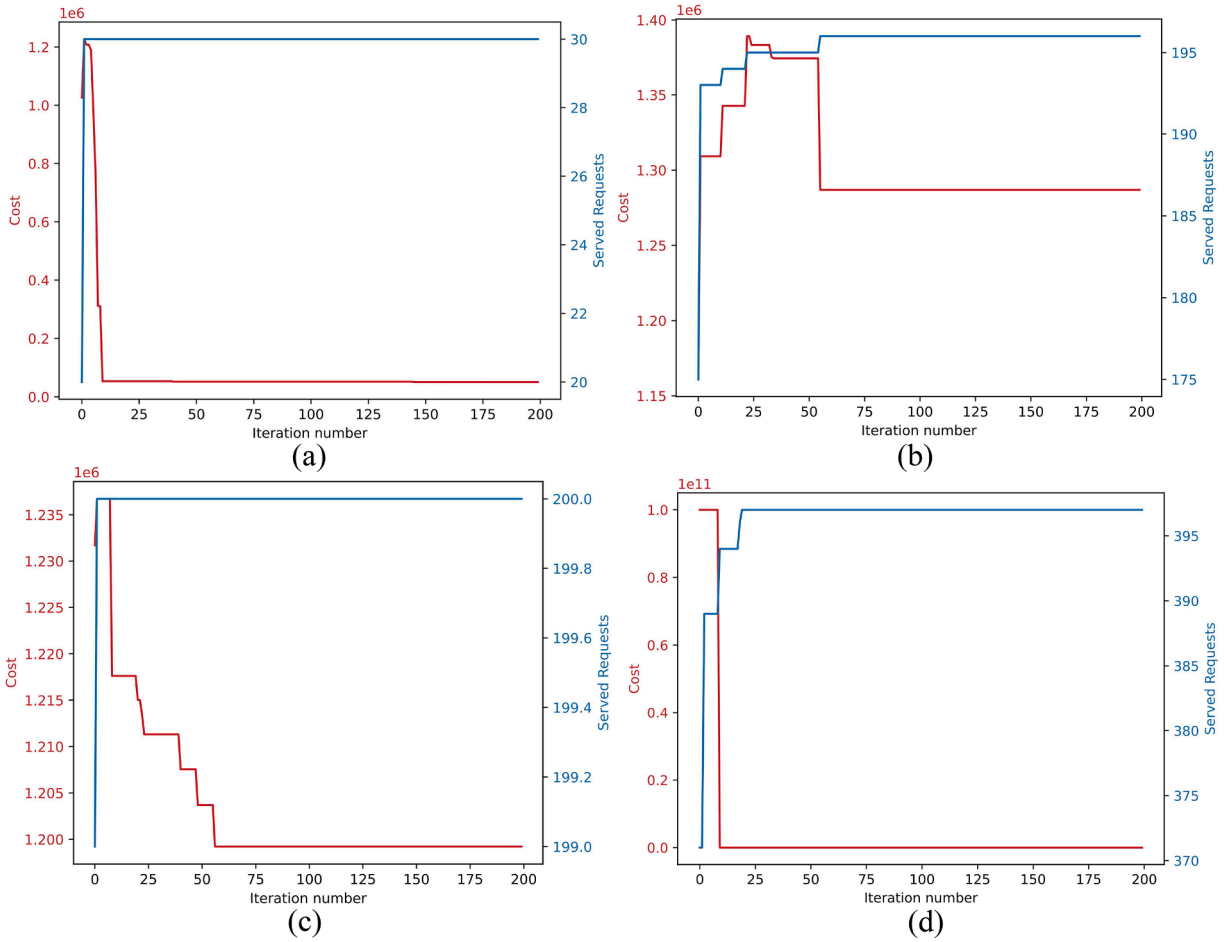

Fig. 13. Convergence of ALNS on different instances.

Table 6
Analysis on ALNS algorithm's stability.

	Total Costs (CNY)										Mean	Std. Dev.	CV
$\|O\|$	1	2	3	4	5	6	7	8	9	10	(CNY)	(CNY)	(%)
5	37,399	37,399	37,399	37,399	37,399	37,399	37,399	37,399	37,399	37,399	37,399	0	0
10	58,423	58,423	58,423	58,423	58,423	58,423	58,423	58,423	58,423	58,423	58,423	0	0
20	97,735	97,735	97,735	97,735	97,735	97,735	97,735	97,735	97,735	97,735	97,735	0	0
30	157,919	157,919	157,919	159,061	158,061	157,919	157,919	158,586	159,061	157,919	158,228	460	0.3
50	252,636	248,634	249,784	250,389	253,013	251,816	247,681	248,292	250,547	251,611	250,440	1750	0.7
100	623,990	624,530	624,686	624,870	622,349	624,653	623,711	625,959	625,973	622,028	624,274	1,249	0.2
200	1,156,912	1,164,581	1,147,664	1,158,272	1,160,824	1,150,044	1,150,044	1,158,236	1,168,953	1,166,852	1,158,238	7331	0.6
400	2,435,806	2,490,096	2,491,945	2,466,783	2,512,111	2,507,832	2,497,840	2,452,511	2,459,963	2,458,198	2,477,308	24610	1.0

$|O|$: number of orders; Mean: average of the 10 runs; Std. Dev.: standard deviation of the 10 runs; CV: Coefficient of variation, CV = Std. Dev. / Mean × 100 %.

set at 50 % each across all orders. The results are presented in Table B.2, which details total costs and five sub-cost components under varying order volumes. To better visualize the cost differences, each cost metric is normalized, and the comparison is illustrated in the radar chart in Fig. 14.

Fig. 14 shows that, except for the 100-order instance, the approach with drones consistently incurs a higher total cost F. This is primarily due to the higher unit transit cost of drones and the fact that F is largely driven by transit cost F_1, which accounts for at least 78 % of the total cost (see Fig. 15). Additionally, drones must be transported to takeoff points by other vehicles, consuming cargo space and increasing vehicle demand. The most pronounced cost differences occur in the 5-order and 400-order instances: in the former, an excess number of drones are transported compared to those actually used; in the latter, drone availability is insufficient

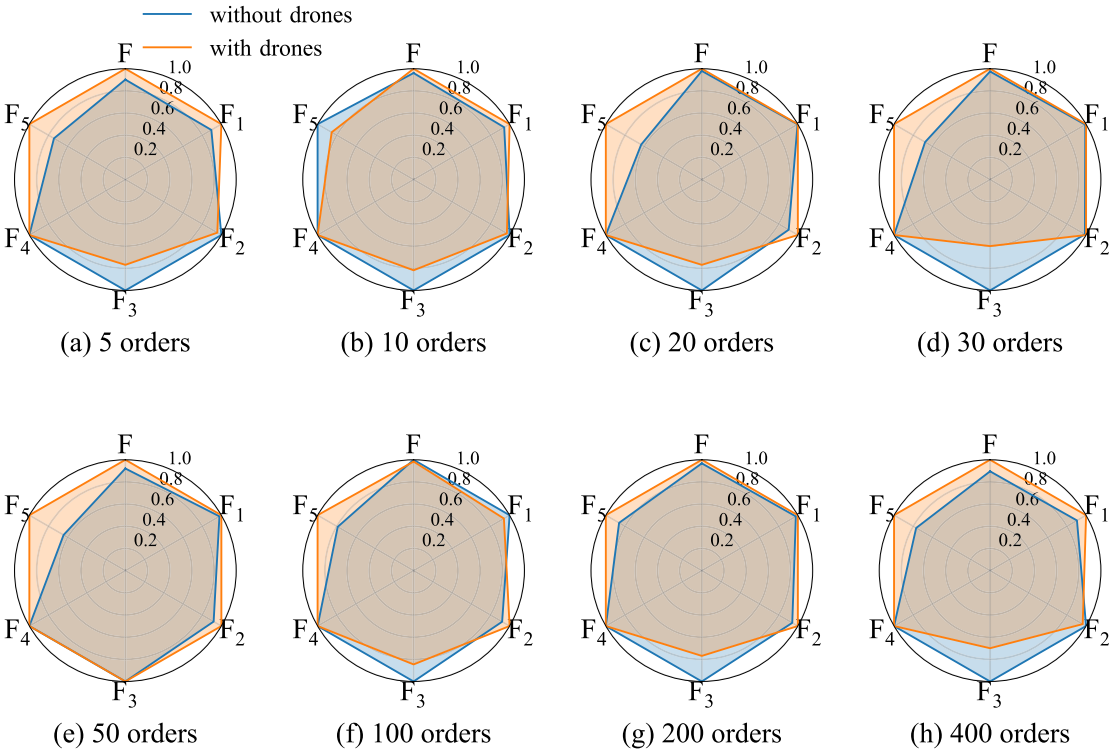

Fig. 14. Radar chart for comparing different unit costs in approaches with and without drones.

to meet demand. However, for order volumes between 10 and 200, the total costs in both models are comparable, indicating that drones are most cost-effective and efficient in medium-scale scenarios.

Despite drones' lower load capacity–which would theoretically require more transfers, the unit transfer cost F_2 remains nearly identical between the approaches with and without drones (Fig. 14), indicating drones' superior transfer efficiency. The approach with drones also achieves a significantly lower unit storage cost F_3, with an average reduction of 23 % compared to the approach without drones. This improvement is attributed to drones' flexible, on-demand operation, enabling faster loading and dispatch. However, except for the 10-order case, the approach with drones consistently incurs a higher unit delay penalty F_5 (Fig. 14). This is because drones are primarily assigned to time-sensitive emergency orders, which have tighter delivery windows and higher associated penalties. Notably, F_5 is the second-largest cost component after transit cost F_1 in the total cost F (Fig. 15), highlighting the importance of time-efficiency management in drone-integrated logistics.

Fig. 16(a) shows that the approach without drones achieves only a 60 % overall service rate for the 5-order scenario and fails entirely to fulfill emergency orders, highlighting its limitations at small scales. Additionally, the service rate for emergency orders consistently lags behind that of normal orders. In contrast, the approach with drones achieves full (100 %) service coverage for 5–30 orders, maintains a high 98 % rate at 50 orders (with 100 % completion of emergency orders), recovers to 100 % at 200 orders, and slightly declines to 87.5 % at 400 orders–suggesting the 400-order instance exceeds system capacity. Moreover, the approach with drones stabilizes the ratio of emergency-to-normal order service rates between 0.86 and 1.0, marking an improvement of over 83 % compared to the traditional model's range of 0–0.89, thereby significantly enhancing emergency order prioritization.

As illustrated in Fig. 16(b), the approach with drones boosts the emergency order service rate by 12–100 % (averaging 45.5 %) and improves normal order service by 0–20 %. This results in an average increase of 26 % in total service rate, with only a 5 % average rise in total cost. Excluding the 400-order case, the cost increase drops to just 4 %, while the service rate improvement reaches 28 %. This favorable trade-off–"low cost increase for high service gain"–underscores the effectiveness and value of drone integration in emergency logistics.

Fig. 17 shows that in the results of the approach without drones, road transport dominates, accounting for 42–68 % of total usage. After introducing drones, their share rises significantly–reaching 42 % at the 50-order scale–surpassing road transport (30 %) for the first time and becoming the primary mode, while trucks are relegated to a supporting role. Notably, rail transport maintains a consistent share across all order volumes in both instances, indicating a stable, rigid demand for rail services.

As illustrated in Fig. 18, the introduction of drones most significantly affects road transport, which sees an average reduction of over 18 %, highlighting direct competition between drones and trucks. In medium- to large-scale scenarios (20–200 orders), the share of road transport drops by more than 20 % on average, demonstrating drones' efficiency and competitiveness at this scale. Rail transport remains constrained by fixed infrastructure, and air transport is primarily used for long-distance, high-priority deliveries,

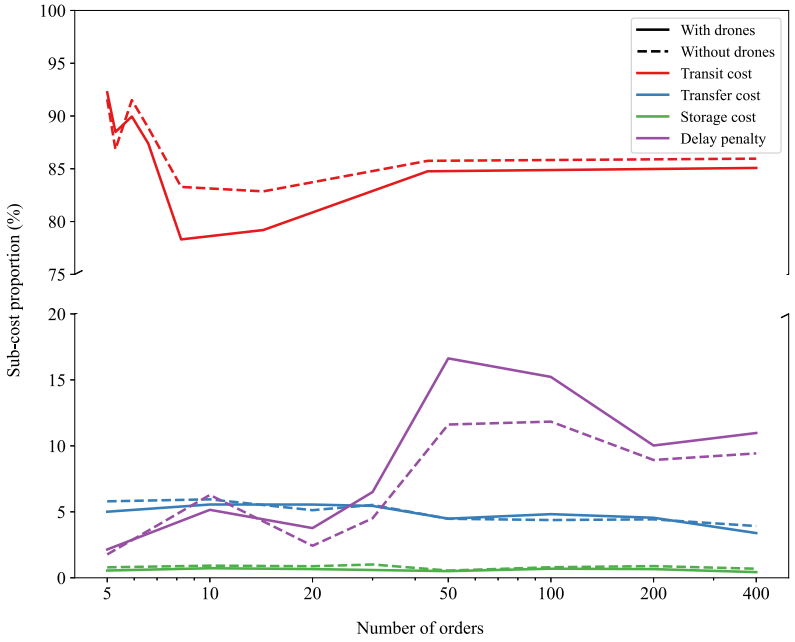

Fig. 15. Sub-cost proportions across varying numbers of orders under approaches with and without drones.

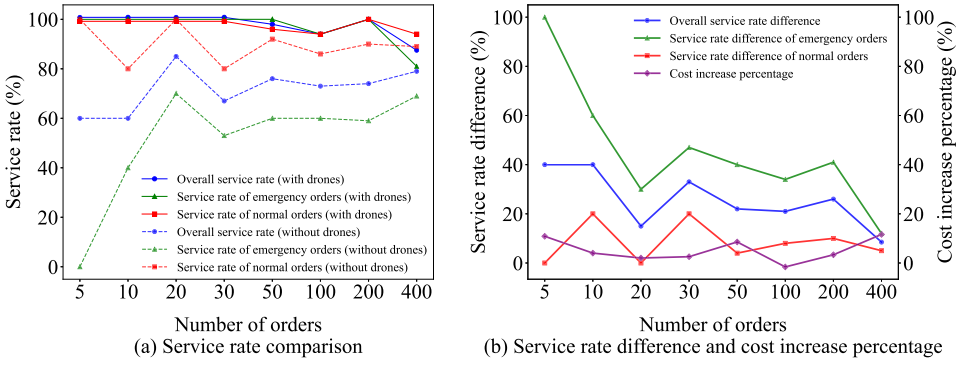

Fig. 16. Comparison of service rates and costs between approachs with and without drones.

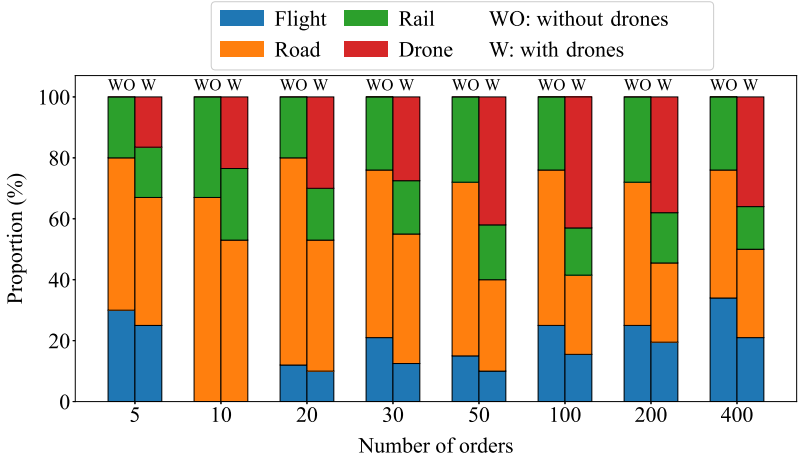

Fig. 17. Transport modes usage proportion comparison between approaches with and without drones.

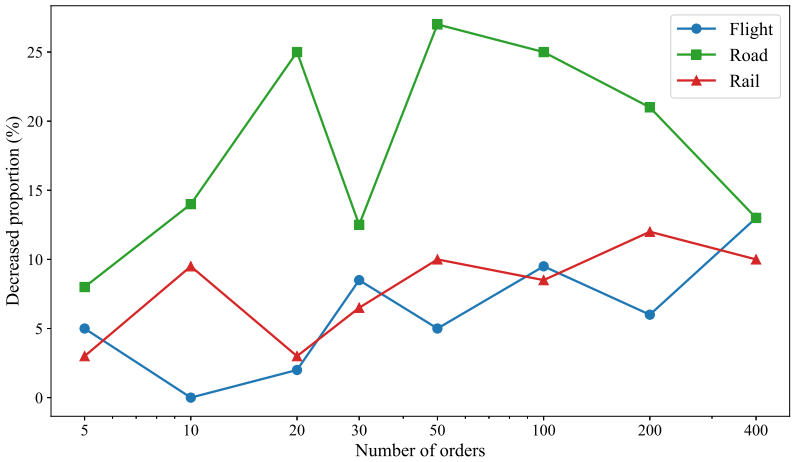

Fig. 18. The decrease proportion of three transport modes after introducing drones.

making both modes more complementary than competitive with drones. The rebound in air transport share at the 400-order level suggests that the system increasingly relies on aircraft when drone capacity becomes insufficient for urgent deliveries.

In summary, introducing drones–despite a modest increase in overall costs–greatly improves service rates, particularly for emergency orders. Drones are especially advantageous for order volumes between 20 and 200, offering a strong balance between cost and efficiency. In disaster-affected regions, drone integration significantly enhances responsiveness. For carriers, drones are most cost-effective for medium-scale instances and help reduce transfer and storage times. Efficient time management is key to minimizing drone-related operational costs. From a governmental perspective, careful planning of the truck-to-drone ratio is essential. In medium-scale scenarios, expanding drone fleet coverage should be prioritized, while in large-scale emergencies, maximizing air transport capacity becomes critical. Across all instances, rail transport should be used to maintain reliable, large-volume supply movement–forming the backbone of a stable and efficient emergency logistics network.

7.4. Performance in dynamic scenario

Section 7.4.1 compares the static transport model with the proposed dynamic model under disruption scenarios. Section 7.4.2 demonstrates that the proposed model maintains good stability and robustness even under numerous sudden events and large-scale network changes.

7.4.1. Comparison of static and dynamic models

We randomly remove a road segment from all paths leading to drone takeoff points, cutting off access for all transport modes in the static model. As a result, drone operations and related order deliveries are completely disabled. In contrast, the dynamic model adapts by reassigning the disruption point as a new takeoff location and replanning routes to ensure order fulfillment. To evaluate performance, unit costs, transport mode shares, and order service rates are analyzed, with orders o_e and o_n each comprising 50 % of total demand. The results, presented in Table B.3, demonstrate the dynamic model's clear advantages in maintaining service continuity. Fig. 19 visualizes these results by normalizing the cost indicators from the table, further highlighting the resilience and effectiveness of the dynamic DMT-Drones model.

Fig. 19 reveals that the dynamic model consistently outperforms the static model in both total unit cost F (3.5–27 % lower) and unit transit cost F_1 (5–29 % lower), primarily due to the static model's inability to handle disruptions. The dynamic model demonstrates the most significant cost differences in large-scale instances (100+ orders: average reduction of 19 % in F and 24 % in F_1), while showing slight improvements in mid-scale instances (10–50 orders: only 5–7 % average reduction). Its lower unit storage cost F_3 highlights the benefits of drones' on-demand flexibility, and the reason for higher delay penalties F_5 is mentioned in Section 7.3.

Fig. 20(a) demonstrates that the dynamic model consistently outperforms the static model in service rate across all instances. For small to medium order volumes (5–30 orders), the dynamic model achieves a 100 % service rate for all order types, while the static model fails to fulfill any emergency orders in the 5-order scenario. As order volumes exceed 50, the dynamic model continues to prioritize emergency orders–even when not all orders are served–whereas the static model shows a steady decline in service performance. Notably, at 400 orders, the dynamic model recovers with a 5 % increase in service rate, while the static model continues to deteriorate, highlighting the dynamic model's superior adaptability in large-scale scenarios.

Fig. 20(b) further illustrates that the dynamic model provides, on average, a 56 % higher emergency order service rate and a 35 % higher overall service rate compared to the static model. The gap in performance for emergency orders remains at least 24 % higher than for normal orders, underscoring the dynamic model's effectiveness in prioritizing time-critical deliveries. When overlaying the cost-saving curve, the dynamic model's advantages peak at 5 and 100 orders, where the highest differences in both cost and service rate are observed.

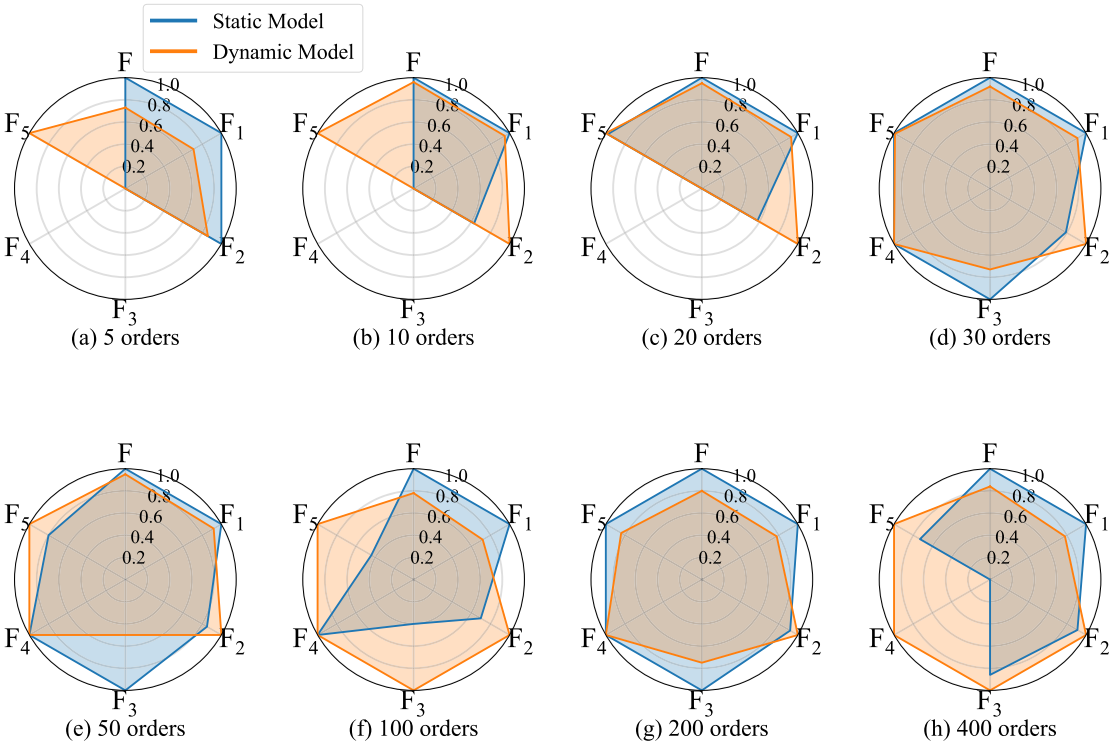

Fig. 19. Radar chart for comparing diverse average cost metrics in static and dynamic models.

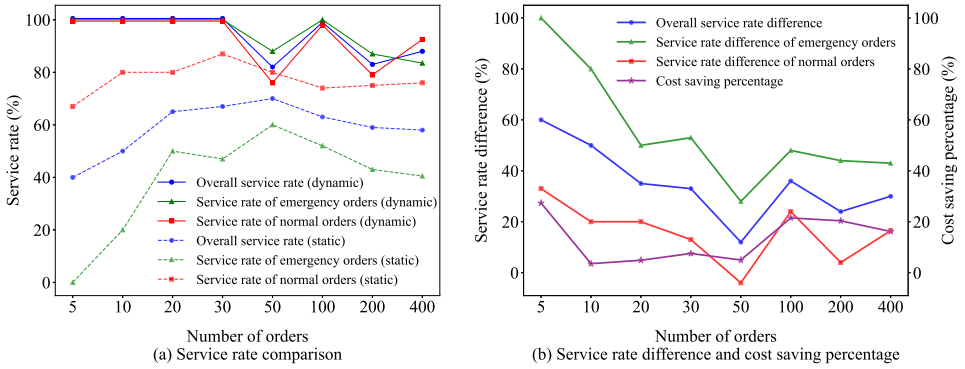

Fig. 20. Comparison of static and dynamic model on order service rates and cost saving under varying number of orders.

Additionally, Fig. 21 offers a visual comparison of the actual routing networks. It clearly shows that the dynamic model successfully navigates unexpected disruptions, completing nearly all deliveries without interruption. In contrast, the static model frequently encounters mid-route failures due to its inability to adapt, further validating the operational superiority of the dynamic model.

Fig. 22 highlights key differences in mode usage between the static and dynamic models. The static model primarily relies on air-road combinations in small-scale (5–10 orders) and large-scale (200–400 orders) scenarios, while road transport dominates medium-scale instances (20–100 orders). In contrast, the dynamic model shifts to air-drone combinations for small-scale cases, drone-road for medium-scale, and a drone-air-road mix for large-scale instances. Rail usage remains consistent across both models, reflecting stable demand. Notably, drone usage shows a strong negative correlation with the number of orders ($r = -0.93$), confirming their scalability limitations in large-scale operations. The dynamic model also demonstrates higher efficiency, requiring only two-thirds of the vehicle growth rate needed by the static model.

Fig. 23 further reveals competitive dynamics between drones and air transport in small- and large-scale cases, with air usage dropping by 19 % in the dynamic model–indicating that drones can effectively substitute air in certain emergency contexts. In medium-scale scenarios, drones primarily replace road transport, resulting in a 27.5 % reduction in truck usage.

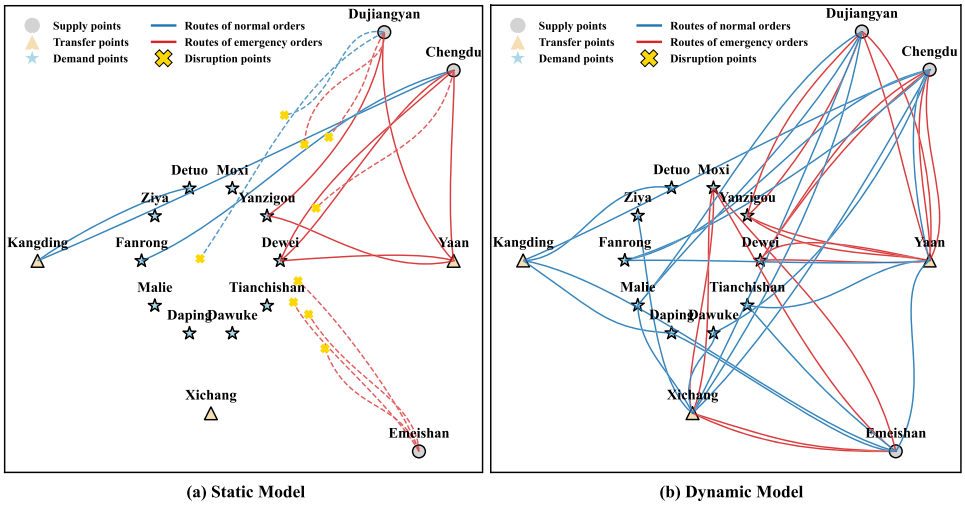

Fig. 21. Comparison of static and dynamic model on transport routes.

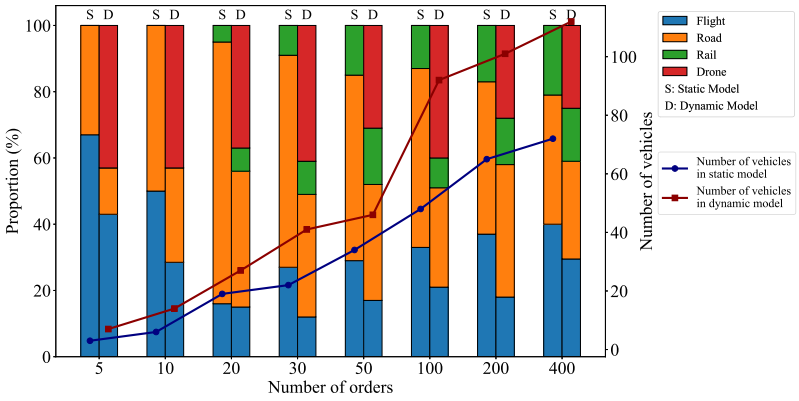

Fig. 22. Comparison of static and dynamic models on vehicle numbers and transportation modes proportion under different order instances.

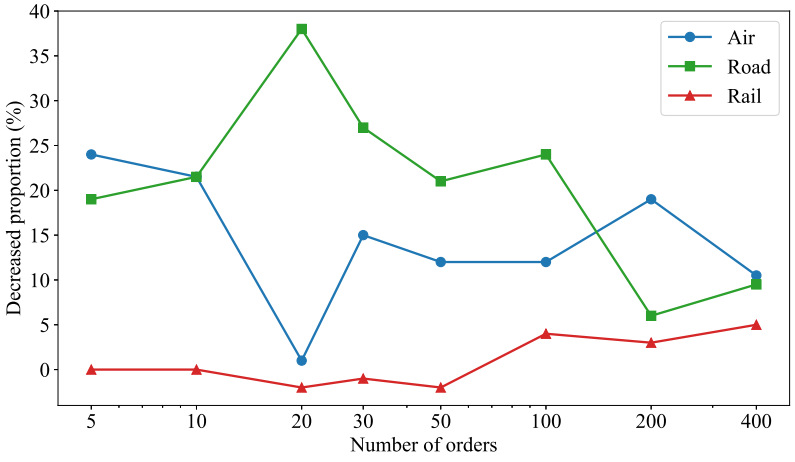

Fig. 23. The decrease proportion of three transport modes compared to the static model.

Table 7
The impact of numerous sudden events and large-scale network changes.

	Unit Costs (CNY/ton/km)						Gap (%)	Time (s)		Service Rate (%)			Replanning effect	
$\|O\|$	F	F_1	F_2	F_3	F_4	F_5	F	Best	Each	Overall	Static	Gap	Influenced	Replanned
Low frequency														
50	1.496	1.337	0.058	0.006	0.000	0.094	–	806.71	10.76	96	56	71	10	8 (80 %)
100	1.445	1.302	0.068	0.008	0.000	0.066	–	1122.46	7.58	93	57	63	23	22 (96 %)
200	1.494	1.355	0.047	0.005	0.000	0.087	–	5388.81	18.33	92	57	61	50	44 (88 %)
400	1.593	1.472	0.040	0.004	0.000	0.076	–	14036.46	23.59	86	55	56	85	76 (89 %)
High frequency														
50	1.517	1.328	0.062	0.007	0.000	0.120	1.4	731.37	11.08	78	56	39	28	19 (68 %)
100	1.456	1.304	0.068	0.010	0.000	0.074	0.8	291.06	2.14	79	56	41	58	43 (74 %)
200	1.513	1.340	0.061	0.006	0.000	0.105	1.3	8306.09	30.20	75	53	39	120	88 (73 %)
400	1.516	1.372	0.052	0.008	0.000	0.084	−4.8	33712.37	62.09	73	52	40	229	163 (71 %)

$|O|$: number of orders; Unit Costs: cost per ton per kilometer; F: total cost, F_1: transit cost, F_2: transfer cost, F_3: storage cost, F_4: waiting cost, F_5: delay penalty; initial: computation time for finding the first feasible solution, Best: computation time for finding the optimal solution; Each: average computation time for each order under each unexpected event; Overall: overall service rate; Static: the service rate under static model; Influenced: the cumulative number of orders affected by unexpected events during transport (allowing multiple counts for the same order due to multiple unexpected events); Replanned: the cumulative number of disrupted orders that were successfully recovered through route re-planning.

In summary, the DMT-Drones model proves essential across all order scales in disaster-affected areas. For carriers, it offers substantial cost savings–especially in small and large-scale scenarios. For government agencies, optimal resource allocation should focus on drone-to-aircraft ratio optimization in extreme-scale instances and on balancing drone and road transport in medium-scale cases, while ensuring continuous and stable use of rail for bulk logistics support.

7.4.2. Performance under numerous sudden events

We conduct a set of comparative experiments under medium- and large-scale scenarios to evaluate the proposed model. These experiments are designed to verify its stability in response to frequent sudden events, as well as its planning accuracy under varying planning horizon lengths and update frequencies. The results, summarized in Table 7, show that the total unit cost under high-frequency disruptions is only 0.8–1.4 % higher than that under low-frequency disruptions for instances with 50, 100, and 200 orders. Notably, for 400-order instances, although some orders are not served, the unit cost is even 4.8 % lower under high-frequency settings. This demonstrates that the proposed model maintains high solution quality and robustness even under intensive disruptions and large-scale conditions.

We have further measured the average computation time required for each order's re-planning iteration. Except for the 400-order case under high-frequency disruptions, all instances complete re-planning within 30 s. For problem sizes under 100 orders, the re-planning time is typically less than 11 s, and in the best case, only 2 s are needed. These results confirm the model's practical applicability and computational efficiency, enabling frequent re-optimization without imposing a significant computational burden.

In terms of service rate, the model achieves 86–96 % under low-frequency disruptions and 73–78 % under high-frequency disruptions. Compared with a static model, the service rate improves by 56–71 % in the low-frequency case and 39–41 % in the high-frequency case. While the margin of improvement narrows as disruption frequency increases, it remains stable across different problem sizes, indicating no sharp degradation and verifying the model's consistency and reliability.

Moreover, we analyze the number of times orders are affected by disruptions and the number of times they are successfully re-planned. These values refer to the number of occurrences rather than unique orders, as individual orders may experience repeated disruptions. This setup reflects a realistic dynamic environment, where both disruption likelihood and re-planning frequency increase in regions closer to the disaster area, resulting in higher update frequency. Under low-frequency disruptions, 80–96 % of affected orders are successfully re-planned, while in high-frequency scenarios, the rate remains at 68–74 %, further confirming the model's adaptability and robustness under dynamic and uncertain conditions.

7.5. Results under heterogeneous cargoes

As shown in Table B.4, to investigate the impact of cargo heterogeneity on our model, we randomly selected 10, 30, 100, and 400 orders from instances, with each order set is further divided into three scenarios: (a) 100 % normal orders (o_n), (b) 20 % emergency orders (o_e) and 80 % normal orders (o_n), and (c) 50 % emergency orders (o_e) and 50 % normal orders (o_n).

As discussed in Sections 7.3 and 7.4.1, Fig. 24 is generated by normalizing the unit costs from Table B.4. The figure reveals that in instances with 30, 100, and 400 orders, Scenario (c) (where emergency orders o_e make up 50 % of all orders) shows significantly higher total unit cost F and transportation cost F_1 compared to Scenarios (a) and (b), with average increases of 19 %/14 % and 17 %/12 %, respectively. These increases are primarily driven by greater drone usage, which is necessitated by the higher proportion of emergency orders. In terms of timeliness, for small-scale instances (10/30 orders), Scenario (c) (with a higher emergency order ratio) has only 24 %/86 % of the F_5 (delay penalty) of Scenario (b), as prioritizing emergency orders reduces delays when capacity is sufficient. However, in over-capacity instances (100/400 orders), Scenario (c)'s F_5 exceeds that of Scenario (b) by 140.5 %/19.5 %,

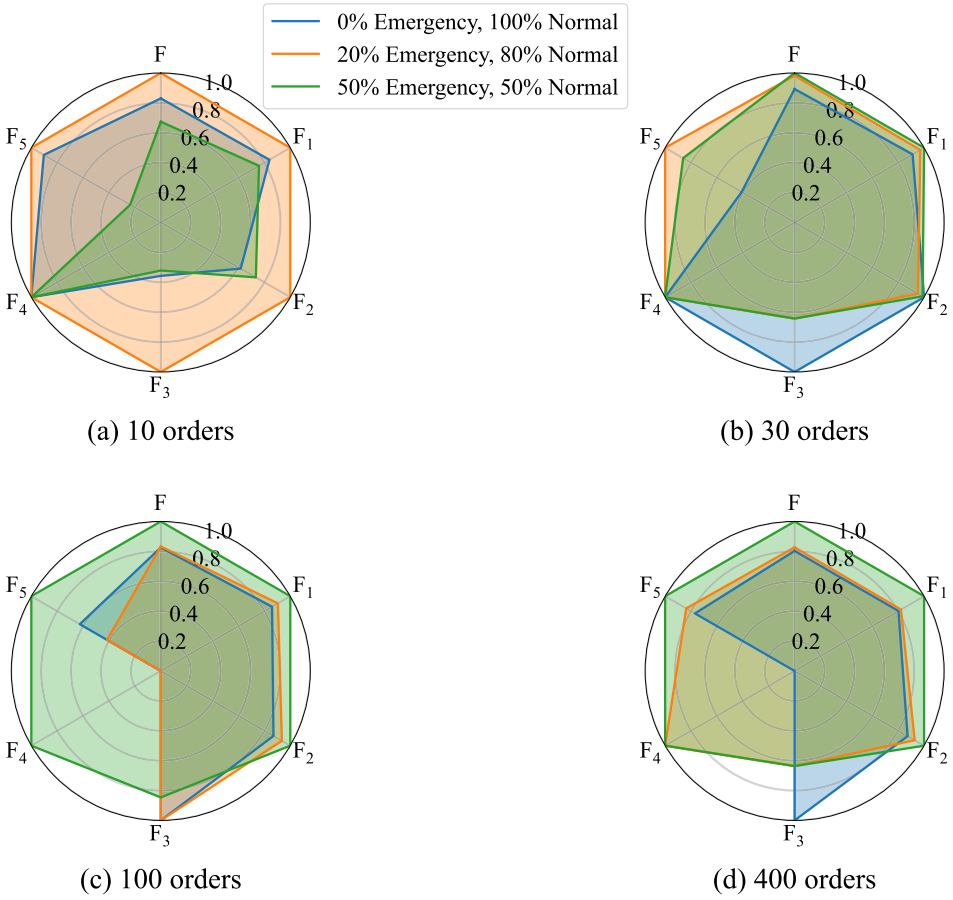

Fig. 24. Radar chart of cargo heterogeneity under different order instances.

due to the growing backlog of emergency orders and escalating penalty costs. Notably, in the 10- and 100-order instances, Scenario (a) (100 % normal orders) exhibits unusually high F_5 values (381 % and 150.5 % higher than Scenario (c) and Scenario (b), respectively), further confirming the timeliness advantage of drones. Additionally, Scenario (c) consistently demonstrates the lowest storage cost F_3, emphasizing the flexibility of drones in optimizing scheduling.

As shown in Fig. 25(a), for small-to-medium order volumes, Scenarios (b) and (c) achieve a 100 % service rate, while Scenario (a) leaves some orders unserved, indicating that the model performs better when emergency orders are included. As order volumes increase to 100–400, Scenario (b) consistently outperforms Scenario (c) in service rate. At 400 orders, Scenario (c) even falls below Scenario (a) due to exceeding drone capacity limits, confirming that drones are unsuitable for large-scale operations. Additionally, higher ratios of emergency orders increase service rate volatility (standard deviation: 6.2 for (c) and 3.1 for (b)), highlighting that cargo heterogeneity amplifies fluctuations.

Fig. 25(b) shows that for the small-scale instance (10 orders), Scenario (c) is optimal, achieving the same service rate as Scenario (b) while reducing costs by 20 % compared to Scenario (a) and 40 % compared to Scenario (b). For medium-scale instances (30 orders), Scenario (b) is preferred despite its higher costs, as emergency logistics prioritizes service rate. In large-scale instances (100–400 orders), Scenario (b) remains optimal, with its service rate improvements outweighing the cost increase, unlike Scenario (c). This analysis provides insights for configuring emergency order ratios across different demand scales.

Due to drones' limited payload capacity and the urgent nature of emergency orders, drones are designated exclusively for transporting emergency orders, resulting in 0 % utilization in Scenario (a), where no emergency demand exists. As shown in Fig. 26(a), the proportion of emergency orders is positively correlated with the total number of utilized vehicles. For example, in a 10-order instance, increasing the share of emergency orders from 0 % to 50 % raises vehicle demand by 30.8 % (from 13 to 17). Similarly, in the 400-order Scenario (c), vehicle demand rises by 70.3 % compared to Scenario (a) (from 91 to 155), highlighting the added logistical complexity that emergency orders introduce. However, vehicle demand growth is not solely driven by emergency proportions: Scenario (b) shows the largest increase (from 15 to 154) when scaling from 10 to 400 orders, as it must simultaneously manage normal deliveries while prioritizing emergency shipments.

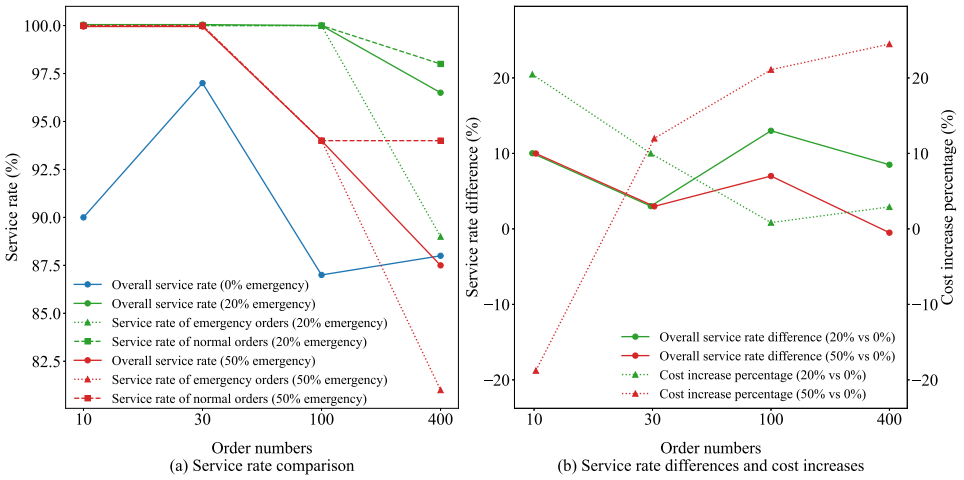

Fig. 25. Impact of cargo heterogeneity on order service rates under diverse order instances.

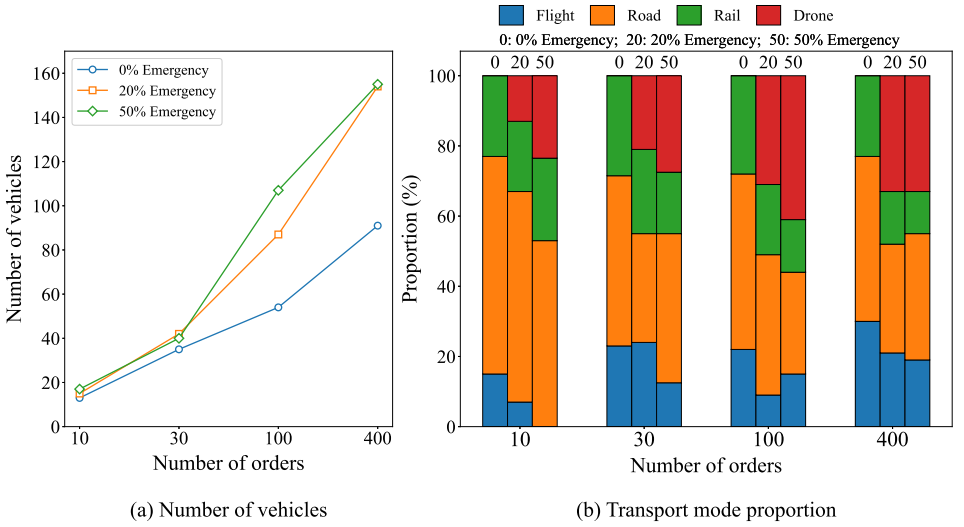

Fig. 26. The impact of cargo heterogeneity on vehicle numbers and transportation modes proportion under different order instances.

Fig. 26(b) shows that the drones' transport share significantly increases with the proportion of emergency orders, averaging 41.5 % higher in Scenario (c) than in Scenario (b). Drones primarily displace road and air transport: in the 100-order instance, increasing the emergency order proportion from 0 % to 50 % reduces road transport share from 50 % to 29 % and air transport from 22 % to 9 %, while drone usage rises to 41 %. This displacement pattern remains consistent across different order volumes. Furthermore, the analysis shows that air transport share grows with increasing order volume across all instances, underscoring its importance for large-scale operations. Road transport declines gradually but rebounds by 7 % at very large scales, maintaining its critical role. Rail transport remains stable, with fluctuations under 6 %, demonstrating its reliability.

In summary, for disaster-affected areas, the model performs best when emergency orders account for around 20 % of total demand. For carriers, the most effective strategy is to handle 50 % emergency orders in small-scale instances while focusing on normal orders in larger scenarios. For governments, the ideal approach is to transport 50 % emergency orders at small scales and maintain 20 % emergency order transport at larger scales. Efficient emergency logistics depends on strategically balancing cargo heterogeneity, order scale, and capacity allocation.

7.6. Sensitivity analysis of key parameters

In this section, we explore the impacts of key parameters using the 50-order instance, namely the speed of vehicles v_k, the unit transit cost of vehicles $c_k^{1'}$, as well as the delay penalty coefficient c_k^5. We evaluate the following performance metrics: unit costs, modal share, and service rate. The detailed benchmark values and sensitivity analysis results of each parameter are provided in Tables A.1, C.5–C.8 in Appendices A and C, respectively.

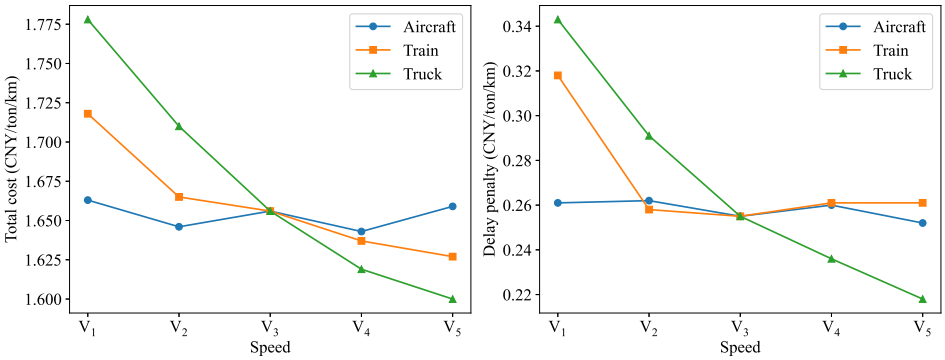

(a) Impact of vehicle speed on total cost (b) Impact of vehicle speed on delay penalty

Fig. 27. Sensitivity analysis of vehicle speed on costs.

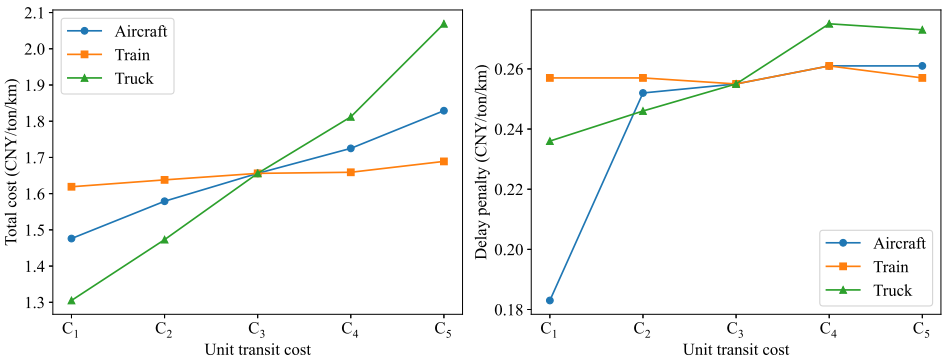

(a) Impact of unit transit cost on total cost (b) Impact of unit transit cost on delay penalty

Fig. 28. Sensitivity analysis of unit transit cost on costs.

Fig. 27 illustrates the changes in total cost and delay penalties for three types of vehicles across five speed scenarios. Instances V1–V5 correspond to penalty levels of 60 %, 80 %, 100 %, 120 %, and 140 % of the benchmark value (V3). In Fig. 27(a), increases in train and truck speeds steadily reduce total cost. This can be attributed to the fact that higher speeds shorten transport time, thereby lowering time-related costs and consequently reducing overall costs. In contrast, the total cost for aircraft fluctuates: as speed increases, the model tends to select aircraft more frequently to expedite delivery, but the high unit transport cost of aircraft can, in some cases, push up total cost. In Fig. 27(b), higher truck speeds consistently reduce delay penalties, indicating that truck acceleration has the most significant effect on reducing delays. For trains, delay penalties drop sharply at first and then level off, suggesting that once train speed reaches a certain threshold, the main bottleneck shifts to other segments (e.g., last-mile delivery), limiting the benefit of further acceleration. Aircraft delay penalties show minor fluctuations, possibly because faster aircraft speeds lead the model to use them more for feasible shipments, but this can postpone some ground-transport tasks for orders that cannot be carried by air, causing slight variations in delay penalties. In summary, under current conditions, increasing truck speed is the most effective way to reduce both total cost and delay penalties. Train acceleration yields substantial early benefits but has an upper limit, while the benefits of increasing aircraft speed are constrained by high operating costs and limited applicability; their advantages become more evident only when delay penalties are weighted more heavily or flight costs are reduced.

Fig. 28 shows the changes in total cost and delay penalties for three types of vehicles under five cost instances. Instances C1–C5 correspond to unit transit cost of 60 %, 80 %, 100 %, 120 %, and 140 % of the benchmark value (C3). In Fig. 28(a), the total cost of three transport modes increases as unit transit rises, with the largest increase observed for trucks, followed by aircraft, and the smallest for trains. This can be attributed to trucks contributing the highest ton-kilometers in the solution, which makes total cost most sensitive to changes in their unit cost. Although aircraft have a high unit cost, their relatively small share of transported volume results in only a moderate impact. In contrast, trains maintain a stable share and have a low unit cost, leading to the smallest increase. In Fig. 28(b), increasing the unit transit cost of aircraft results in a rise in the overall delay penalty, as reduced aircraft usage lowers the average transport speed and causes more delays. The delay penalty for trucks also increases, while that for trains changes little, reflecting their relatively fixed and specialized role in the transport system. In summary, reducing truck unit costs is the most effective approach to curbing total cost growth. Controlling aircraft unit costs is most beneficial for maintaining timeliness. By contrast, adjustments to train unit costs have a comparatively limited effect on both indicators.

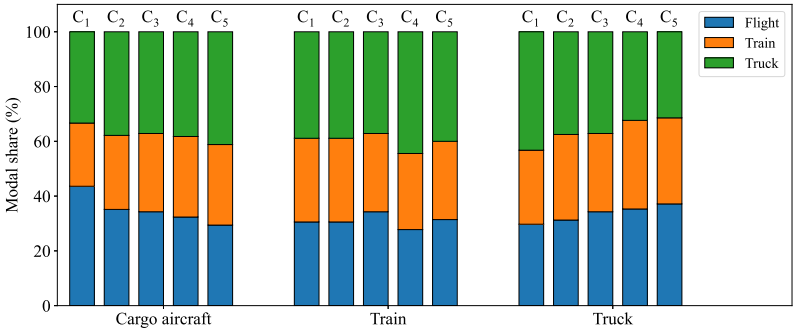

Fig. 29. Sensitivity analysis of unit transit cost on transport modes proportion.

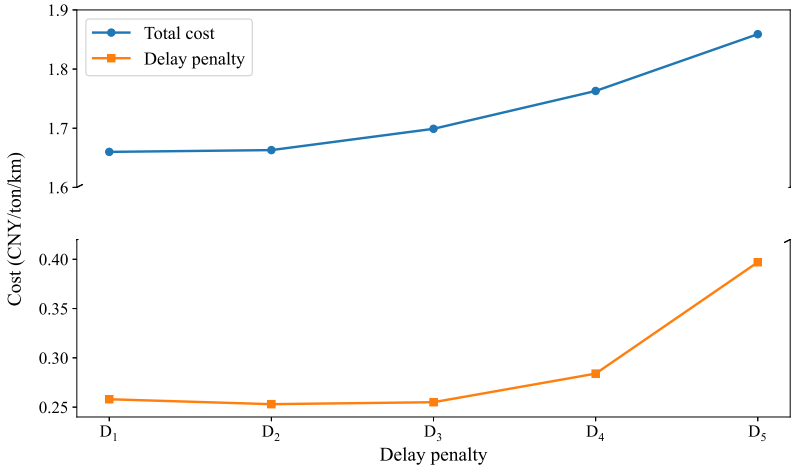

Fig. 30. Sensitivity analysis of delay penalty coefficient.

Fig. 29 shows the changes in the proportion of three vehicle types under five instances with different unit transit costs. The results indicate that when the unit transport cost of aircraft increases, its share decreases significantly, with the model shifting more toward trucks and trains to reduce costs. Changes in train costs lead to almost no change in the shares of different vehicles, indicating that the train's role in the transport network is relatively fixed. When truck costs increase, their share declines, and the model tends to use aircraft as a substitute for trucks, with the proportion of aircraft eventually surpassing that of trucks. Overall, the sensitivity of mode share to cost changes is highest for aircraft, followed by trucks, and lowest for trains.

Fig. 30 illustrates the changes in total cost and delay penalties under five delay penalty coefficient instances. Instances D1–D5 correspond to penalty levels of 60 %, 80 %, 100 %, 120 %, and 140 % of the benchmark value (D3). It should be noted that, the delay penalty coefficient is independent of the transport mode used and is instead determined by the intrinsic characteristics of each order. Based on the urgency of the orders (i.e., the size of the time window), the coefficients are classified into three levels: 90, 50, and 30. Delay penalties show a slight decline between instances D1 and D2. This is because, when the penalty coefficient increases from a low level, the model shifts toward faster modes (e.g., aircraft) to reduce delays, and in this range the reduction in actual delays outweighs the magnifying effect of the higher coefficient of delay penalty. Once the coefficient reaches the benchmark (D3) and beyond, the penalty term dominates the objective function. Even after switching to faster modes, unavoidable delays incur disproportionately high penalties, which substantially raise total costs. Consequently, both delay penalties and total costs accelerate in growth. In summary, the delay penalty weight exhibits a threshold effect: moderate increases can reduce delays via mode switching, whereas exceeding the threshold leads to significant cost increase.

Fig. 31 illustrates the impact of unit transit cost for drones on the model. Fig. 31(a) shows that within the range of 60–120 % of the benchmark (C1-C4), total cost increases slightly while the delay penalty remains largely unchanged; however, when the cost rises to 140 % of the benchmark (C5), the delay penalty surges sharply, and total cost also increases significantly. This pattern can be explained by the modal share presented in Fig. 31(b). When the cost is below a certain threshold, the solution consistently employs drones to maintain high timeliness, with vehicle allocation remaining nearly unchanged, thus keeping delays at a low level. Once the cost exceeds the threshold, the model substantially reduces drone usage, and helicopters and trucks cannot match the flexibility, adaptability, and other advantages of drones, leading to a sharp increase in delays.

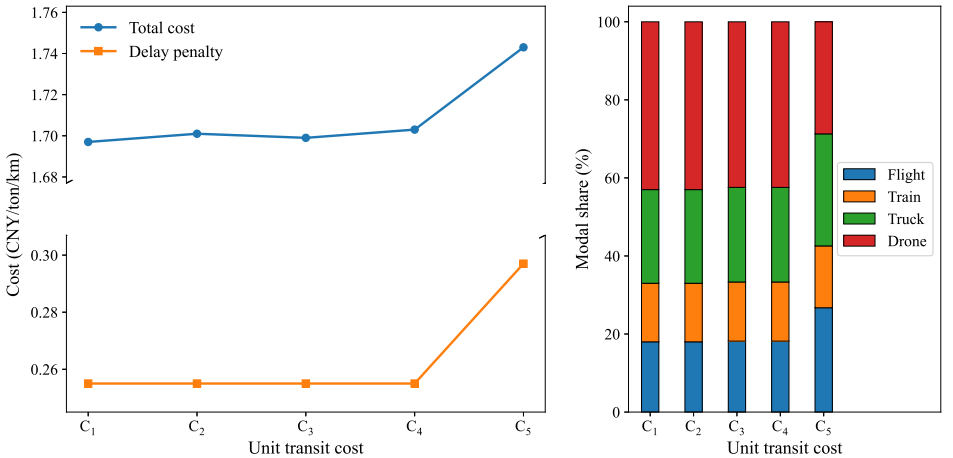

(a) Impact of the drones unit transit cost on total cost and delay penalty

(b) Impact of the drones unit transit cost on modal share

Fig. 31. Sensitivity analysis of the unit transit cost of drones.

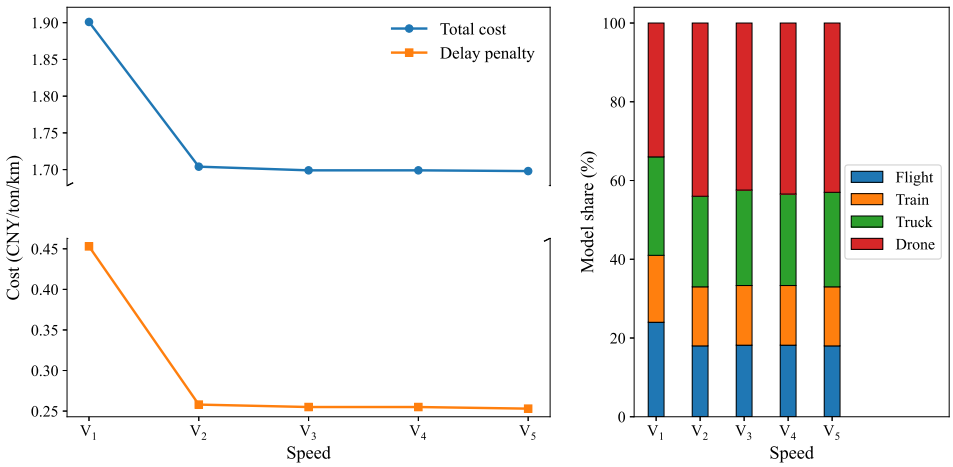

(a) Impact of the drones speed on total cost and delay penalty

(b) Impact of the drones speed on modal share

Fig. 32. Sensitivity analysis of the speed of drones.

Similarly, Fig. 32 shows the impact of drone speed on the transport system. When speed is above a certain threshold, the model still uses drones, and both modal share and total cost remain essentially unchanged. When speed falls below the threshold, the model stops using drones, and delay penalties and total costs rise sharply. In summary, under the current network and constraints, drones provide a substantial contribution to delay reduction. Their adoption, however, depends on maintaining unit costs and transport speeds within specific threshold levels.

8. Conclusion and future directions

To address the challenges of limited flexibility and inadequate emergency response capabilities in emergency logistics, this study proposes a dynamic multimodal transport planning approach integrating four modes: trains, trucks, aircraft, and drones. Drones are distinguished by their dual-role capability, functioning both as cargo transported by other modes and as independent carriers, which enhances responsiveness and adaptability within multimodal systems. A MIP model is developed, supported by a customized ALNS algorithm to ensure computational efficiency. The ALNS framework incorporates specialized operators and performance enhancement strategies, while a rolling horizon approach is adopted for dynamic planning. The model captures critical features including multimodal coordination, dynamic re-planning, cargo heterogeneity, and the dual roles of drones, with simultaneous routing of vehicles and orders to maximize operational flexibility.

The model demonstrates strong performance across multiple objectives and scenarios. Comparisons with a commercial solver (Gurobi) validate the ALNS algorithm's superiority in reducing computation time. Its adaptability to dynamic environments is val-

idated through tests involving sudden road segment disruptions, highlighting improvements in flexibility and transport efficiency. Comparative analyses show that integrating drones significantly enhances overall system performance, reducing transport time and cost while improving operational resilience.

In practice, the proposed model provides a valuable decision-support tool for logistics planners, emergency response coordinators, and transport operators, enabling real-time optimization of multimodal transport systems. By improving efficiency and adaptability, it offers a practical and effective solution for managing real-world emergency logistics operations. Specifically, after a natural disaster, emergency management agencies can use this model to quickly generate an initial relief delivery plan based on available post-disaster information (e.g., known road availability, supply locations, and urgent demand points). As new disruptions occur (e.g., infrastructure damage), the model can be re-invoked with updated inputs to dynamically re-optimize vehicle and drone routes, resource allocation, and timing decisions. This continuous adjustment process supports resilient response operations throughout the relief period. Moreover, the model incorporates real-world operational constraints, including heterogeneous vehicle fleets, mode-specific routing limitations (e.g., fixed routes for rail and aircraft, flexible for trucks and drones), and cargo heterogeneity (e.g., prioritizing emergency supplies over normal items). These practical considerations enable the model to address common challenges in disaster relief, such as limited vehicle availability, heterogeneous urgent demand, last-mile accessibility issues, and infrastructure disruptions. The model's outputs can inform different stakeholders (e.g., emergency response centers, local governments, and logistics operators) by offering guidance for allocation, dispatching, and real-time coordination under high-stress conditions.

The proposed DMT-drones approach offers an effective optimization framework tailored specifically for emergency logistics, demonstrating strong potential for cost reduction, efficiency improvement, and higher service rates by dynamically integrating drones with multimodal transport. From the results, we obtain the following insights:

1. For disaster-affected areas, the model optimizes emergency order allocation to ensure efficient relief distribution, with drone integration significantly improving service rates for critical supplies, particularly in small- to medium-scale scenarios.
2. For carriers, the model enables cost savings by dynamically optimizing delivery routes in real-time scenarios, strategically deploying drones for 50 % of emergency orders in small-scale scenarios. Effective time management is critical to reducing drones' operational costs and streamlining their seamless integration into existing logistics systems.
3. For governments, the optimal strategy is to transport 50 % of emergency orders in small-scale scenarios and maintain a 20 % allocation in other contexts. Resource allocation should be balanced through a "drones + trucks" network while ensuring rail system stability. In medium-scale cases, expanding drone fleets enhances coverage, whereas large-scale emergencies benefit from maximizing air transport capacity, fostering efficient and flexible emergency logistics.

Future research in multimodal transport planning for emergency logistics should focus on managing uncertainty, applying more advanced dynamic planning approaches, promoting collaborative planning, and ensuring equitable resource distribution. Addressing uncertainty requires the development of robust and stochastic optimization models that incorporate real-time data, such as road conditions, weather changes, and resource availability, to enhance system adaptability and resilience. Despite the demonstrated effectiveness, the rolling horizon approach may suffer from reduced accuracy when facing extremely frequent disruptions and multiple sources of uncertainty, which future research may address through more intelligent methods such as data-driven modeling, prediction-based optimization, or adaptive buffering strategies. Collaborative planning frameworks involving government agencies, private logistics providers, and humanitarian organizations are crucial for improving coordination, resource sharing, and dynamic allocation across multiple modes. Furthermore, future studies should integrate equity into resource allocation models to ensure vulnerable populations receive timely and adequate support.

CRediT authorship contribution statement

Yimeng Zhang: Writing – review & editing, Writing – original draft, Visualization, Validation, Supervision, Software, Resources, Methodology, Investigation, Funding acquisition, Formal analysis, Conceptualization; **Shuyang Zhu:** Writing – review & editing, Writing – original draft, Visualization, Validation, Formal analysis, Conceptualization; **Kaiyu Pu:** Visualization, Validation, Software, Formal analysis, Conceptualization; **Hang Cui:** Writing – original draft, Visualization, Conceptualization; **Mi Gan:** Supervision, Funding acquisition; **Xiaobo Liu:** Supervision, Funding acquisition; **Ruixue Ai:** Visualization, Conceptualization.

Data availability

The data is available at the following link: https://github.com/ShuyangZhu/DMT-Drones_original_data.

Declaration of competing interest

The authors declare that they have no known competing financial interests or personal relationships that could have appeared to influence the work reported in this paper.

Acknowledgments

This work is supported by the National Natural Science Foundation of China (Nos. 52402521, 52372306, 52232011, U2568219). This work is also partly co-funded by Sichuan Natural Science Foundation (No. 2025NSFSC1969), Hebei Natural Science Founda-

tion (No. G2024105007), Fundamental Research Funds for the Central Universities of China (No. 2682025CX056), and Sichuan Science and Technology Program "PIANJI" Project (No. 2025HJPJ0011).

Appendix A. Parameters used in this paper

All parameters are referenced from Guo et al. (2024), Li and Zhang (2020), Wang et al. (2023), Chen et al. (2023), as shown in Table A.1.

Table A.1
Parameters used in the paper.

parameter	value	parameter	value	parameter	value	parameter	value
c^1_{truck}	50.584	c^1_{train}	7.755	$c^1_{aircraft}$	217.5	c^1_{drone}	47.5
$c^{1'}_{truck}$	0.6323	$c^{1'}_{train}$	0.1551	$c^{1'}_{aircraft}$	1.45	$c^{1'}_{drone}$	1.45
c^2_{truck}	2	c^1_{train}	7.5	$c^2_{aircraft}$	7.5	c^2_{drone}	7.5
c^3_{truck}	1.5	c^3_{train}	1.5	$c^3_{aircraft}$	1.5	c^3_{drone}	1.5
c^4_{truck}	1.5	c^4_{train}	1.5	$c^4_{aircraft}$	1.5	c^4_{drone}	1.5
v_{truck}	80 km/h	v_{train}	50 km/h	$v_{aircraft}$	150 km/h	v_{drone}	150 km/h

Appendix B. Results of numerical experiments

Tables B.2–B.4 present the results for models with and without drones, static and dynamic approaches, and scenarios with heterogeneous cargoes, respectively.

Table B.2
Comparison of approaches with and without drones.

	Unit Costs (CNY/ton/km)						# of	Modal Share (%)				CPU (s)		Service Rate(%)		
$\|O\|$	F	F_1	F_2	F_3	F_4	F_5	Vehicles	flight	road	rail	drone	initial	best	overall	o_e	o_n
Without Drones																
5	1.639	1.501	0.095	0.013	0.001	0.029	10	30	50	20	0	1.97	1.97	60	0	100
10	1.194	1.037	0.071	0.011	0.001	0.075	12	0	67	33	0	10.20	10.20	60	40	80
20	1.483	1.357	0.076	0.013	0.001	0.036	25	12	68	20	0	18.99	98.77	85	70	100
30	1.485	1.320	0.082	0.015	0.001	0.067	29	21	55	24	0	25.21	262.77	67	53	80
50	1.274	1.061	0.057	0.007	0.001	0.148	46	15	57	28	0	91.23	325.32	76	60	92
100	1.622	1.344	0.071	0.013	0.001	0.192	67	25	51	24	0	161.29	5684.76	73	60	86
200	1.467	1.258	0.065	0.013	0.001	0.131	76	25	47	28	0	1360.40	20668.99	74	59	90
400	1.453	1.249	0.057	0.010	0.001	0.137	88	34	42	24	0	3658.48	37516.09	79	69	89
With Drones																
5	1.817	1.676	0.091	0.010	0.001	0.039	12	25	42	17	17	2.20	2.20	100	100	100
10	1.242	1.099	0.069	0.009	0.001	0.064	17	0	53	23.5	23.5	10.41	30.62	100	100	100
20	1.513	1.361	0.084	0.010	0.001	0.057	30	10	43	17	30	18.34	68.08	100	100	100
30	1.523	1.331	0.083	0.009	0.001	0.099	40	12.5	42.5	17.5	27.5	24.57	244.67	100	100	100
50	1.383	1.083	0.062	0.007	0.001	0.230	67	10	30	18	42	113.95	2439.92	98	100	96
100	1.596	1.264	0.077	0.011	0.001	0.243	103	15.5	26	15.5	43	230.60	13620.35	94	94	94
200	1.516	1.285	0.069	0.010	0.001	0.152	130	19	26	16	38	1385.80	10895.03	100	100	100
400	1.622	1.380	0.055	0.007	0.001	0.178	139	21	29	14	36	3553.82	5103.33	88	81	94

$|O|$: number of orders; Unit Costs: cost per ton per kilometer; F: total cost, F_1: transit cost, F_2: transfer cost, F_3: storage cost, F_4: waiting cost, F_5: delay penalty; flight: proportion of orders served by flight, road: proportion of orders served by road, rail: proportion of orders served by rail, drone: proportion of orders served by drone; initial: computation time for finding the first feasible solution, best: computation time for finding the optimal solution; overall: overall service rate; o_e: emergency orders; o_n: normal orders.

Table B.3
Comparison of static and dynamic models.

	Unit Costs (CNY/ton/km)						# of	Modal Share (%)				CPU (s)		Service Rate (%)		
$\|O\|$	F	F_1	F_2	F_3	F_4	F_5	Vehicles	flight	road	rail	drone	initial	best	overall	o_e	o_n
Static Model																
5	2.973	2.902	0.070	0.000	0.000	0.000	3	67	33	0	0	0.53	0.53	40	0	67
10	2.005	1.967	0.038	0.000	0.000	0.000	6	50	50	0	0	1.68	1.68	50	20	80
20	2.047	1.902	0.030	0.000	0.000	0.115	19	16	79	5	0	6.48	46.97	65	50	80
30	2.065	1.816	0.050	0.011	0.002	0.186	22	27	64	9	0	19.39	405.13	67	47	87
50	1.749	1.594	0.040	0.002	0.001	0.112	34	29	56	15	0	51.51	857.83	70	60	80
100	1.739	1.641	0.038	0.002	0.001	0.057	48	33	54	13	0	161.88	6018.12	63	52	74
200	1.694	1.491	0.047	0.008	0.001	0.146	65	37	46	17	0	1464.46	48846.08	59	43	75
400	1.711	1.526	0.041	0.006	0.000	0.137	72	40	39	21	0	5396.71	5887.24	58	40.5	76
Dynamic Model																
5	2.160	2.070	0.060	0.000	0.000	0.030	7	43	14	0	43	1.49	1.49	100	100	100
10	1.934	1.864	0.060	0.000	0.000	0.010	14	28.5	28.5	0	43	3.19	4.86	100	100	100
20	1.947	1.778	0.052	0.000	0.000	0.117	27	15	41	7	37	12.56	57.57	100	100	100
30	1.909	1.652	0.063	0.008	0.002	0.185	41	12	37	10	41	30.54	773.20	100	100	100
50	1.662	1.472	0.047	0.001	0.001	0.140	46	17	35	17	31	60.08	640.67	82	88	76
100	1.365	1.177	0.054	0.005	0.001	0.129	92	21	30	9	40	185.85	3871.15	99	100	98
200	1.349	1.168	0.051	0.006	0.001	0.123	101	18	40	14	28	1039.90	28230.50	83	87	79
400	1.434	1.191	0.045	0.007	0.002	0.188	112	29.5	29.5	16	25	2591.46	2591.46	88	83.5	92.5

$|O|$: number of orders; Unit Costs: cost per ton per kilometer; F: total cost, F_1: transit cost, F_2: transfer cost, F_3: storage cost, F_4: waiting cost, F_5: delay penalty; flight: proportion of orders served by flight, road: proportion of orders served by road, rail: proportion of orders served by rail, drone: proportion of orders served by drone; initial: computation time for finding the first feasible solution, best: computation time for finding the optimal solution; overall: overall service rate; o_e: emergency orders; o_n: normal orders.

Table B.4
Results under heterogeneous cargoes.

	Proportion (%)		Unit Costs (CNY/ton/km)						# of	Modal Share (%)				CPU (s)		Service Rate (%)		
$\|O\|$	o_e	o_n	F	F_1	F_2	F_3	F_4	F_5	Vehicles	flight	road	rail	drone	initial	best	overall	o_e	o_n
	0	100	1.529	1.216	0.058	0.010	0.001	0.244	13	15	62	23	0	6.95	294.54	90	–	90
10	20	80	1.842	1.449	0.094	0.028	0.001	0.270	15	7	60	20	13	4.82	4.82	100	100	100
	50	50	1.242	1.099	0.069	0.009	0.001	0.064	17	0	53	23.5	23.5	10.41	30.62	100	100	100
	0	100	1.360	1.213	0.084	0.014	0.001	0.047	35	23	48.5	28.5	0	35.85	476.26	97	–	97
30	20	80	1.496	1.292	0.080	0.009	0.001	0.115	42	24	31	24	21	39.41	630.17	100	100	100
	50	50	1.523	1.331	0.083	0.009	0.001	0.099	40	12.5	42.5	17.5	27.5	24.57	244.67	100	100	100
	0	100	1.318	1.086	0.067	0.013	0.000	0.152	54	22	50	28	0	333.12	13237.27	87	–	87
100	20	80	1.329	1.143	0.072	0.013	0.000	0.101	87	9	40	20	31	484.19	7003.74	100	100	100
	50	50	1.596	1.264	0.077	0.011	0.001	0.243	107	15	29	15	41	230.60	13620.35	94	94	94
	0	100	1.303	1.107	0.048	0.011	0.000	0.137	91	30	47	23	0	5897.47	117201.61	88	–	88
400	20	80	1.341	1.134	0.051	0.007	0.001	0.149	154	21	31	15	33	5766.93	29761.39	96.5	89	98
	50	50	1.622	1.380	0.055	0.007	0.001	0.178	155	19	36	12	32	3553.82	5103.33	87.5	81	94

$|O|$: number of orders; Unit Costs: costs per ton per km; o_e: emergency orders; o_n: normal orders; F: total cost, F_1: transit cost, F_2: transfer cost, F_3: storage cost, F_4: waiting cost, F_5: delay penalty; flight: proportion of orders served by flight, road: proportion of orders served by road, rail: proportion of orders served by rail, drone: proportion of orders served by drone; initial: computation time for finding the first feasible solution, best: computation time for finding the optimal solution; overall: overall service rate; o_e: emergency orders; o_n: normal orders.

Appendix C. Sensitivity analysis results

Tables C.5–C.8 present the sensitivity analysis results of the speed of vehicles, the unit transit cost of vehicles, the delay penalty coefficient, and the impact of drones' cost and speed, respectively.

Table C.5
Sensitivity analysis of the speed of vehicles.

	Unit Costs (CNY/ton/km)						Number of Vehicles			CPU (s)		Service Rate
V	F	F_1	F_2	F_3	F_4	F_5	Flight	Train	Truck	Initial	Best	(%)
Cargo aircraft												
V_1^f	1.663	1.339	0.054	0.008	0.001	0.261	12	10	12	42.82	71.40	100
V_2^f	1.646	1.323	0.053	0.008	0.001	0.262	10	10	18	41.36	1647.56	100
V_3^f	1.656	1.338	0.054	0.008	0.000	0.255	12	10	13	40.28	76.68	100
V_4^f	1.643	1.322	0.053	0.008	0.001	0.260	10	10	17	37.42	212.65	100
V_5^f	1.659	1.344	0.054	0.008	0.001	0.252	12	10	15	40.60	77.84	100
Train												
V_1^r	1.718	1.339	0.053	0.008	0.000	0.318	10	10	16	51.11	400.50	100
V_2^r	1.665	1.345	0.054	0.008	0.000	0.258	11	10	14	38.29	792.23	100
V_3^r	1.656	1.338	0.054	0.008	0.000	0.255	12	10	13	40.28	76.68	100
V_4^r	1.637	1.315	0.053	0.008	0.001	0.261	10	10	17	40.17	2236.82	100
V_5^r	1.627	1.306	0.053	0.008	0.001	0.261	10	10	15	39.15	2117.86	100
Truck												
V_1^h	1.778	1.371	0.056	0.007	0.001	0.343	13	10	11	45.11	53.60	100
V_2^h	1.710	1.355	0.056	0.008	0.001	0.291	13	10	14	38.22	424.47	100
V_3^h	1.656	1.338	0.054	0.008	0.000	0.255	12	10	13	40.28	76.68	100
V_4^h	1.619	1.322	0.053	0.008	0.001	0.236	10	10	19	39.18	2637.75	100
V_5^h	1.600	1.321	0.053	0.008	0.001	0.218	10	10	16	38.62	720.27	100

$|O|$: number of orders; V: the speed state of the vehicles; V_1^k: the speed of vehicles decreases 40 %; V_2^k: the speed of vehicles decreases 20 %; V_3^k: benchmark; V_4^k: the speed of vehicles increases 20 %; V_5^k: the speed of vehicles increases 40 %; Unit Costs: cost per ton per kilometer; F: total cost, F_1: transit cost, F_2: transfer cost, F_3: storage cost, F_4: waiting cost, F_5: delay penalty; initial: computation time for finding the first feasible solution, best: computation time for finding the optimal solution.

Table C.6
Sensitivity analysis of the unit transit cost of vehicles.

	Unit Costs (CNY/ton/km)						Number of Vehicles			CPU (s)		Service Rate
C	F	F_1	F_2	F_3	F_4	F_5	Flight	Train	Truck	Initial	Best	(%)
Cargo aircraft												
C_1^f	1.476	1.222	0.063	0.007	0.001	0.183	17	9	13	99.95	718.97	100
C_2^f	1.579	1.263	0.056	0.008	0.001	0.252	13	10	14	38.91	637.27	100
C_3^f	1.656	1.338	0.054	0.008	0.000	0.255	12	10	13	40.28	76.68	100
C_4^f	1.725	1.402	0.053	0.008	0.001	0.261	11	10	13	44.62	326.14	100
C_5^f	1.829	1.510	0.049	0.007	0.001	0.261	10	10	14	44.62	418.96	100
Train												
C_1^r	1.619	1.297	0.057	0.008	0.001	0.257	11	11	14	44.73	878.98	100
C_2^r	1.638	1.316	0.057	0.008	0.001	0.257	11	11	14	44.76	69.21	100
C_3^r	1.656	1.338	0.054	0.008	0.000	0.255	12	10	13	40.28	76.68	100
C_4^r	1.659	1.338	0.053	0.008	0.001	0.261	10	10	16	46.58	1518.30	100
C_5^r	1.689	1.370	0.054	0.008	0.001	0.257	11	10	14	44.03	334.76	100
Truck												
C_1^h	1.305	1.015	0.048	0.006	0.001	0.236	11	10	16	42.27	1856.72	100
C_2^h	1.473	1.168	0.050	0.007	0.001	0.246	10	10	12	52.69	197.33	100
C_3^h	1.656	1.338	0.054	0.008	0.000	0.255	12	10	13	40.28	76.68	100
C_4^h	1.812	1.468	0.059	0.009	0.001	0.275	12	11	11	39.33	1655.09	100
C_5^h	2.069	1.703	0.077	0.014	0.001	0.273	13	11	11	61.99	67.96	100

$|O|$: number of orders; C: the cost state of the vehicles; C_1^k: the unit transit cost of vehicles decreases 40 %; C_2^k: the unit transit cost of vehicles decreases 20 %; C_3^k: benchmark; C_4^k: the unit transit cost of vehicles increases 20 %; C_5^k: the unit transit cost of vehicles increases 40 %; Unit Costs: cost per ton per kilometer; F: total cost, F_1: transit cost, F_2: transfer cost, F_3: storage cost, F_4: waiting cost, F_5: delay penalty; initial: computation time for finding the first feasible solution, best: computation time for finding the optimal solution.

Table C.7
Sensitivity analysis of the delay penalty coefficient.

	Unit Costs (CNY/ton/km)						# of	Modal Share (%)				CPU (s)		Service Rate
D	F	F_1	F_2	F_3	F_4	F_5	Vehicles	Flight	Train	Truck	Drone	initial	best	(%)
D_1	1.660	1.326	0.067	0.009	0.001	0.258	59	19	17	20	44	57.53	70.46	100
D_2	1.663	1.328	0.072	0.009	0.001	0.253	67	16	15	30	39	54.94	3430.39	100
D_3	1.699	1.365	0.071	0.008	0.001	0.255	66	18	15	24	42	48.64	991.10	100
D_4	1.763	1.401	0.070	0.007	0.001	0.284	59	22	17	29	49	49.10	2985.04	100
D_5	1.859	1.385	0.069	0.007	0.001	0.397	66	18	15	26	41	48.20	569.46	100

$|O|$: number of orders; D: the delay penalty coefficient state; D_1: the delay penalty coefficient decreases 40 %; D_2: the delay penalty coefficient decreases 20 %; D_3: benchmark; D_4: the delay penalty coefficient increases 20 %; D_5: the delay penalty coefficient increases 40 %; Unit Costs: cost per ton per kilometer; F: total cost, F_1: transit cost, F_2: transfer cost, F_3: storage cost, F_4: waiting cost, F_5: delay penalty; flight: proportion of orders served by flight, road: proportion of orders served by road, rail: proportion of orders served by rail, drone: proportion of orders served by drone; initial: computation time for finding the first feasible solution, best: computation time for finding the optimal solution.

Table C.8
Sensitivity analysis of drones' cost and speed.

	Unit Costs (CNY/ton/km)						# of	Modal Share (%)				CPU (s)		Service Rate
D	F	F_1	F_2	F_3	F_4	F_5	Vehicles	Flight	Train	Truck	Drone	initial	best	(%)
Unit transit cost														
C_1^u	1.697	1.362	0.072	0.008	0.001	0.255	67	18	15	24	43	48.01	256.10	100
C_2^u	1.701	1.366	0.072	0.008	0.001	0.255	67	18	15	24	43	50.34	394.59	100
C_3^u	1.699	1.365	0.071	0.008	0.001	0.255	66	18	15	24	42	48.64	991.10	100
C_4^u	1.703	1.368	0.072	0.008	0.001	0.255	66	18	15	24	42	49.68	279.23	100
C_5^u	1.743	1.364	0.074	0.008	0.001	0.297	63	27	16	29	29	48.02	549.13	100
Speed														
V_1^u	1.901	1.367	0.072	0.008	0.001	0.453	59	24	17	25	34	48.14	142.03	100
V_2^u	1.704	1.366	0.072	0.008	0.001	0.258	66	18	15	23	44	48.64	247.08	100
V_3^u	1.699	1.365	0.071	0.008	0.001	0.255	66	18	15	24	42	48.64	991.10	100
V_4^u	1.699	1.364	0.071	0.008	0.001	0.255	65	18	15	23	43	48.00	1243.16	100
V_5^u	1.698	1.364	0.072	0.008	0.001	0.253	67	18	15	24	43	51.27	267.06	100

$|O|$: number of orders; C: the cost state of the drones; C_1^u: the unit transit cost of drones decreases 40 %; C_2^u: the unit transit cost of drones decreases 20 %; C_3^u: benchmark; C_4^u: the unit transit cost of drones increases 20 %; C_5^u: the unit transit cost of drones increases 40 %; V: the speed state of the drones; V_1^u: the speed of drones decreases 40 %; V_2^u: the speed of drones decreases 20 %; V_3^u: benchmark; V_4^u: the speed of drones increases 20 %; V_5^u: the speed of drones increases 40 %; Unit Costs: cost per ton per kilometer; F: total cost, F_1: transit cost, F_2: transfer cost, F_3: storage cost, F_4: waiting cost, F_5: delay penalty; flight: proportion of orders served by flight, road: proportion of orders served by road, rail: proportion of orders served by rail, drone: proportion of orders served by drone; initial: computation time for finding the first feasible solution, best: computation time for finding the optimal solution.

References

Abdelgawad, H., Abdulhai, B., 2009. Emergency evacuation planning as a network design problem: a critical review. Transp. Lett. 1 (1), 41–58.

Agatz, N., Bouman, P., Schmidt, M., 2018. Optimization approaches for the traveling salesman problem with drone. Transp. Sci. 52 (4), 965–981.

Anuar, W.K., Lee, L.S., Seow, H.-V., Pickl, S., 2022. A multi-depot dynamic vehicle routing problem with stochastic road capacity: an MDP model and dynamic policy for post-decision state rollout algorithm in reinforcement learning. Mathematics 10 (15), 2699.

Azzalini, A., Capitanio, A., 1999. Statistical applications of the multivariate skew normal distribution. J. R. Stat. Soc. 61 (3), 579–602.

Barbarosoglu, G., Arda, Y., 2004. A two-stage stochastic programming framework for transportation planning in disaster response. J. Oper. Res. Soc. 55, 43–53.

Beiki Ashkezari, A., Zokaee, M., Rabbani, E., Rabbani, M., Aghsami, A., 2024. A scenario-based game theory integrating with a location-allocation-routing problem in a pre-and post-disaster humanitarian logistics network under uncertainty. J. Model. Manag. 19 (5), 1686–1718.

Cao, B., Glover, F., 2010. Creating balanced and connected clusters to improve service delivery routes in logistics planning. J. Syst. Sci. Syst. Eng. 19, 453–480.

Chen, Z., Zhang, Z., Bian, Z., Dai, L., Hu, H., 2023. Subsidy policy optimization of multimodal transport on emission reduction considering carrier pricing game and shipping resilience: a case study of shanghai port. Ocean Coast. Manag. 243, 106760.

Clark, A., Culkin, B., 2013. A network transshipment model for planning humanitarian relief operations after a natural disaster. In: Decision Aid Models for Disaster Management and Emergencies. Springer, pp. 233–257.

Cunha, C.B., Massarotto, D.F., Fornazza, S.L., Mendes, A.B., 2024. An ALNS metaheuristic for the family multiple traveling salesman problem. Comput. Oper. Res. 169, 106750.

Danloup, N., Allaoui, H., Goncalves, G., 2018. A comparison of two meta-heuristics for the pickup and delivery problem with transshipment. Comput. Oper. Res. 100, 155–171.

Ertem, M.A., Akdogan, M.A., Kahya, M., 2022. Intermodal transportation in humanitarian logistics with an application to a turkish network using retrospective analysis. Int. J. Disaster Risk Reduct. 72, 102828.

Fikar, C., Gronalt, M., Hirsch, P., 2016. A decision support system for coordinated disaster relief distribution. Expert Syst. Appl. 57, 104–116.

de Freitas, J.C., Penna, P. H.V., 2020. A variable neighborhood search for flying sidekick traveling salesman problem. Int. Trans. Oper. Res. 27 (1), 267–290.

Gao, X., Jin, X., Zheng, P., Cui, C., 2021. Multi-modal transportation planning for multi-commodity rebalancing under uncertainty in humanitarian logistics. Adv. Eng. Inf. 47, 101223.

Ghilas, V., Demir, E., Van Woensel, T., 2016. An adaptive large neighborhood search heuristic for the pickup and delivery problem with time windows and scheduled lines. Comput. Oper. Res. 72, 12–30.

Gómez-Lagos, J., Candia-Véjar, A., Encina, F., 2021. A new truck-drone routing problem for parcel delivery services aided by parking lots. IEEE Access 9, 11091–11108.

Guo, F., Xu, Y., Huang, Z., Wu, Y., 2024. Collaborative optimization of routing and storage strategy of multi-period multimodal transport in an uncertain environment. Comput. Oper. Res. 167, 106676.

Ha, Q.M., Deville, Y., Pham, Q.D., Hà, M.H., 2020. A hybrid genetic algorithm for the traveling salesman problem with drone. J. Heuristics 26, 219–247.

Haghani, A., Oh, S.-C., 1996. Formulation and solution of a multi-commodity, multi-modal network flow model for disaster relief operations. Transp. Res. Part A 30 (3), 231–250.

Haghani, S.-C. O.A., 1997. Testing and evaluation of a multi-commodity multi-modal network flow model for disaster relief management. J. Adv. Transp. 31 (3), 249–282.

Hakami, A., Kumar, A., Shim, S.J., Nahleh, Y.A., 2013. Application of soft systems methodology in solving disaster emergency logistics problems. Int. J. Ind. Manuf. Eng. 7 (12), 2470–2477.

Hu, Z.-H., 2011. A container multimodal transportation scheduling approach based on immune affinity model for emergency relief. Expert Syst. Appl. 38 (3), 2632–2639.

Huang, J.-S., Huang, Y.-C., Wang, Y.-S., Lien, Y.-N., 2011. Design of a contingency communication network. In: Submitted to 13th Asia–Pacific Network Operations and Management Symposium, pp. 21–23.

Jiang, Y., Yuan, Y., 2019. Emergency logistics in a large-scale disaster context: achievements and challenges. Int. J. Environ. Res. Public Health 16 (5), 779.

Li, D., Ignatius, J., Wang, D., Yin, Y., Cheng, T., 2024. A branch-and-price-and-cut algorithm for the truck-drone routing problem with simultaneously delivery and pickup. Nav. Res. Logist. (NRL) 71 (2), 241–285.

Li, L., Zhang, X., 2020. Reducing CO_2 emissions through pricing, planning, and subsidizing rail freight. Transp. Res. Part D 87, 102483.

Liu, Y., Lei, H., Wu, Z., Zhang, D., 2019. A robust model predictive control approach for post-disaster relief distribution. Comput. Ind. Eng. 135, 1253–1270.

Lu, C.-C., Ying, K.-C., Chen, H.-J., 2016. Real-time relief distribution in the aftermath of disasters–a rolling horizon approach. Transp. Res. Part E 93, 1–20.

Maghfiroh, M. F.N., Hanaoka, S., 2020. Multi-modal relief distribution model for disaster response operations. Prog. Disaster Sci. 6, 100095.

Majidi, S., Hosseini-Motlagh, S.-M., Ignatius, J., 2018. Adaptive large neighborhood search heuristic for pollution-routing problem with simultaneous pickup and delivery. Soft Comput. 22, 2851–2865.

Masson, R., Lehuédé, F., Péton, O., 2013. An adaptive large neighborhood search for the pickup and delivery problem with transfers. Transp. Sci. 47 (3), 344–355.

Meng, L., Wang, X., He, J., Han, C., Hu, S., 2023. A two-stage chance constrained stochastic programming model for emergency supply distribution considering dynamic uncertainty. Transp. Res. Part E 179, 103296.

Moshref-Javadi, M., Hemmati, A., Winkenbach, M., 2020. A truck and drones model for last-mile delivery: a mathematical model and heuristic approach. Appl. Math. Model. 80, 290–318.

Murray, C.C., Chu, A.G., 2015. The flying sidekick traveling salesman problem: optimization of drone-assisted parcel delivery. Transp. Res. Part C 54, 86–109.

Murray, C.C., Raj, R., 2020. The multiple flying sidekicks traveling salesman problem: parcel delivery with multiple drones. Transp. Res. Part C 110, 368–398.

Nedjati, A., 2017. Humanitarian Logistics: Optimization Techniques for Emergency Preparedness and Post-Earthquake Response. Ph.D. thesis. Eastern Mediterranean University EMU-Doğu Akdeniz Üniversitesi (DAÜ).

Otto, A., Agatz, N., Campbell, J., Golden, B., Pesch, E., 2018. Optimization approaches for civil applications of unmanned aerial vehicles (UAVs) or aerial drones: a survey. Networks 72 (4), 411–458.

Özdamar, L., Ekinci, E., Küçükyazici, B., 2004. Emergency logistics planning in natural disasters. Ann. Oper. Res. 129, 217–245.

Peng, W., Wang, D., Yin, Y., Cheng, T., 2025. Multi-agent deep reinforcement learning-based truck-drone collaborative routing with dynamic emergency response. Transp. Res. Part E 195, 103974.

Pisinger, D., Ropke, S., 2007. A general heuristic for vehicle routing problems. Comput. Oper. Res. 34 (8), 2403–2435.

Poikonen, S., Golden, B., 2020. Multi-visit drone routing problem. Comput. Oper. Res. 113, 104802.

Qu, Y., Bard, J.F., 2012. A GRASP with adaptive large neighborhood search for pickup and delivery problems with transshipment. Comput. Oper. Res. 39 (10), 2439–2456.

Rodríguez-Espíndola, O., Dey, P., Albores, P., Chowdhury, S., 2023. Sustainability and intermodality in humanitarian logistics: a two-stage multi-objective programming formulation. Ann. Oper. Res. 346, 1–30.

Rojas Viloria, D., Solano-Charris, E.L., Muñoz-Villamizar, A., Montoya-Torres, J.R., 2021. Unmanned aerial vehicles/drones in vehicle routing problems: a literature review. Int. Trans. Oper. Res. 28 (4), 1626–1657.

Ropke, S., Pisinger, D., 2006. An adaptive large neighborhood search heuristic for the pickup and delivery problem with time windows. Transp. Sci. 40 (4), 455–472.

Ruan, J., Chan, F. T.S., Zhao, X., 2018. Re-planning the intermodal transportation of emergency medical supplies with updated transfer centers. Sustainability 10 (8), 2827.

Salmerón, J., Apte, A., 2010. Stochastic optimization for natural disaster asset prepositioning. Prod. Oper. Manag. 19 (5), 561–574.

Schermer, D., Moeini, M., Wendt, O., 2019. A matheuristic for the vehicle routing problem with drones and its variants. Transp. Res. Part C 106, 166–204.

Shi, Y., Yang, J., Han, Q., Song, H., Guo, H., 2024. Optimal decision-making of post-disaster emergency material scheduling based on helicopter–truck–drone collaboration. Omega 127, 103104.

Souto, L., Parisio, A., Taylor, P.C., 2024. Mpc-based framework incorporating pre-disaster and post-disaster actions and transportation network constraints for weather-resilient power distribution networks. Appl. Energy 362, 123013.
Sumalee, A., Pan, T., Zhong, R., Uno, N., Indra-Payoong, N., 2013. Dynamic stochastic journey time estimation and reliability analysis using stochastic cell transmission model: algorithm and case studies. Transp. Res. Part C 35, 263–285.
The International Disaster Database, 2025. 2024 disasters in numbers. https://www.emdat.be.
Tu, P.A., Dat, N.T., Dung, P.Q., 2018. Traveling salesman problem with multiple drones. In: Proceedings of the 9th International Symposium on Information and Communication Technology, pp. 46–53.
Vásquez, S.A., Angulo, G., Klapp, M.A., 2021. An exact solution method for the TSP with drone based on decomposition. Comput. Oper. Res. 127, 105127.
Veysmoradi, D., Vahdani, B., Farhadi Sartangi, M., Mousavi, S.M., 2018. Multi-objective open location-routing model for relief distribution networks with split delivery and multi-mode transportation under uncertainty. Sci. Iran. 25 (6), 3635–3653.
Vitoriano, B., Ortuno, T., Tirado, G., 2009. Hads, a goal programming-based humanitarian aid distribution system. J. Multi-Criteria Decis. Anal. 16 (1-2), 55–64.
Wan, H., Liu, W., Shi, Q., Zhang, Y., Wang, Y., Zhang, S., 2022. Multi-time-step rolling optimization strategy for post-disaster emergency recovery in distribution system based on model predictive control. CSEE J. Power Energy Syst. 11 (1), 243–254.
Wang, F., Li, H., Xiong, H., 2025. Truck–drone routing problem with stochastic demand. Eur. J. Oper. Res. 322 (3), 854–869.
Wang, L., Song, J., Shi, L., 2015. Dynamic emergency logistics planning: models and heuristic algorithm. Optim. Lett. 9, 1533–1552.
Wang, Z., Sheu, J.-B., 2019. Vehicle routing problem with drones. Transp. Res. Part B 122, 350–364.
Wang, Z., Zhang, D., Tavasszy, L., Fazi, S., 2023. Integrated multimodal freight service network design and pricing with a competing service integrator and heterogeneous shipper classes. Transp. Res. Part E 179, 103290.
Wikipedia, 2024. 2022 luding earthquake — Wikipedia, the free encyclopedia. https://en.wikipedia.org/w/index.php?title=2022_Luding_earthquake. [Online; accessed 10-December-2024].
Wikipedia, 2025. 2025 mokwa flood — Wikipedia, the free encyclopedia. [Online; accessed 20-July-2025]. https://en.wikipedia.org/w/index.php?title=2025_Mokwa_flood.
Wolfinger, D., 2021. A large neighborhood search for the pickup and delivery problem with time windows, split loads and transshipments. Comput. Oper. Res. 126, 105110.
Wu, J., Wang, X.-Y., Tian, A.-Q., Du, Z.-G., Yang, Z.-J., 2024. A hybrid meta-heuristic approach for emergency logistics distribution under uncertain demand. IEEE Access 12, 135701–135729.
Xin, X., Wang, S., Zhang, T., 2025. Truck-drone supported humanitarian relief logistics network design: a two-stage distributionally robust optimization approach. Transp. Res. Part C 178, 105231.
Xiong, X., Zhao, F., Wang, Y., Wang, Y., 2019. Research on the model and algorithm for multimodal distribution of emergency supplies after earthquake in the perspective of fairness. Math. Probl. Eng. 2019, 1–12.
Xu, Z., Zheng, C., Zheng, S., Ma, G., Chen, Z., 2024. Multimodal transportation route optimization of emergency supplies under uncertain conditions. Sustainability 16 (24), 10905.
Yi, W., Kumar, A., 2007. Ant colony optimization for disaster relief operations. Transp. Res. Part E 43 (6), 660–672.
Yin, Y., Li, D., Wang, D., Yu, Y., Cheng, T., 2025. Truck-drone pickup and delivery service optimization with availability profiles. Nav. Res. Logist. (NRL) 72 (4), 534–565.
Yin, Y., Qing, L., Wang, D., Cheng, T., Ignatius, J., 2024a. Exact solution method for vehicle-and-drone cooperative delivery routing of blood products. Comput. Oper. Res. 164, 106559.
Yin, Y., Xu, X., Wang, D., Yu, Y., Cheng, T., 2024b. Two-stage recoverable robust optimization for an integrated location–allocation and evacuation planning problem. Transp. Res. Part B 182, 102906.
Yin, Y., Yang, Y., Yu, Y., Wang, D., Cheng, T., 2023. Robust vehicle routing with drones under uncertain demands and truck travel times in humanitarian logistics. Transp. Res. Part B 174, 102781.
Zhang, J., Liu, H., Yu, G., Ruan, J., Chan, F. T.S., 2019. A three-stage and multi-objective stochastic programming model to improve the sustainable rescue ability by considering secondary disasters in emergency logistics. Comput. Ind. Eng. 135, 1145–1154.
Zhang, L., Lu, J., 2024. Optimizing oil spill emergency logistics: a time-varying multi-resource collaborative scheduling model. Environ. Sci. Pollut. Res. 31 (2), 2773–2801.
Zhang, Y., Guo, W., Negenborn, R.R., Atasoy, B., 2022a. Synchromodal transport planning with flexible services: mathematical model and heuristic algorithm. Transp. Res. Part C 140, 103711.
Zhang, Y., Li, X., Van Hassel, E., Negenborn, R.R., Atasoy, B., 2022b. Synchromodal transport planning considering heterogeneous and vague preferences of shippers. Transp. Res. Part E 164, 102827.
Zhang, Y., Tan, X., Gan, M., Liu, X., Atasoy, B., 2025. Operational synchromodal transport planning methodologies: review and roadmap. Transp. Res. Part E 194, 103915.
Zhang, Z., Zhu, C., Liu, K., Wang, Q., 2022c. Bi-level optimal scheduling of emergency materials considering multimodal transport. Eng. Lett. 30 (2), 494–506.
Zhou, H., Qin, H., Cheng, C., Rousseau, L.-M., 2023. An exact algorithm for the two-echelon vehicle routing problem with drones. Transp. Res. Part B 168, 124–150.
Zhu, J., Huang, J., Liu, D., Han, J., 2008. Resources allocation problem for local reserve depots in disaster management based on scenario analysis. In: The 7th International Symposium on Operations Research and its Applications. Lijiang, China, pp. 395–407.